TOPBP1/Dpb11 Controls DNA Repair Through the Coordinated Recruitment of 53BP1/Rad9

Yi Liu[1,#], Jose Renato Cussiol[1,#], Diego Dibitetto[2,#], Jennie Rae Sims[1], Shyam Twayana[2], Robert Weiss[3], Raimundo Freire[4], Federica Marini[2], Achille Pellicioli[2,§] and Marcus Bustamante Smolka[1,§*]

[1] Department of Molecular Biology and Genetics, Weill Institute for Cell and Molecular Biology, Cornell University, Ithaca, NY 14853

[2] Department of Biosciences, University of Milan, 20133, Milano, Italy

[3] Department of Biomedical Sciences, Cornell University, Ithaca, NY 14853

[4] Unidad de Investigación, Hospital Universitario de Canarias, Instituto de Tecnologias Biomedicas, 38320 Tenerife, Spain

[#] Equal contribution

[§] Co-last author

* Correspondence: mbs266@cornell.edu

Character count: 39,689

Summary

DNA repair by homologous recombination (HR) is crucial for preventing genomic instability and cancer. Here, Liu *et al.* uncover a conserved role for the Dpb11/TOPBP1 scaffold in mediating a phosphorylation-regulated circuitry for HR control. The findings have implications to mechanistically understand tumorigenesis upon *BRCA1* deficiency.

Abbreviations used: 9-1-1, Rad9–Hus1–Rad1; B3/4-Rad9, Dpb11$^{BRCT3/4}$-Rad9 chimera; ChIP, chromatin immunoprecipitation; CTR, constitutive TOPBP1-interacting region; DOX, doxycycline; DSB, double-strand break; HR, homologous recombination; HU, hydroxyurea; MBD, minimal multi-BRCT domain; MMS, methyl methanesulfonate; NHEJ, non-homologous end joining; PARP, poly(ADP-ribose) polymerase; RPA, replication protein A; SILAC, Stable isotope labeling with amino acids in cell culture; SSA, single strand annealing; ssDNA, single-stranded DNA; TOPBP1, topoisomerase IIβ–binding protein 1.

Abstract

Genome maintenance and cancer suppression require homologous recombination (HR) DNA repair. In yeast and mammals, the scaffold protein TOPBP1^{Dpb11} has been implicated in HR, although its precise function and mechanism of action remain elusive. Here we show that yeast Dpb11 plays antagonistic roles in recombination control through regulated protein interactions. Dpb11 mediates opposing roles in DNA end resection by coordinating both stabilization and exclusion of Rad9 from DNA lesions. The Mec1 kinase promotes the pro-resection function of Dpb11 by mediating its interaction with the Slx4 scaffold. Human TOPBP1^{Dpb11} engages in interactions with the anti-resection factor 53BP1 and the pro-resection factor BRCA1, suggesting that TOPBP1 also mediates opposing functions in HR control. Hyper-stabilization of the 53BP1-TOPBP1 interaction enhances the recruitment of 53BP1 to nuclear foci in S-phase, resulting in impaired HR and the accumulation of chromosomal aberrations. Our results support a model in which TOPBP1^{Dpb11} plays a conserved role in mediating a phospho-regulated circuitry for the control of recombinational DNA repair.

Introduction

The proper repair of double strand breaks (DSBs) that occur during DNA replication is heavily dependent on error-free homologous recombination (HR) (Heyer, 2015; Schwartz and Heyer, 2011). However, DSBs may also be repaired by the direct ligation of DNA ends through non-homologous end joining (NHEJ). Because of the risk of ligating wrong ends and/or deleting DNA sequences, NHEJ is considered an error-prone repair mechanism. During DNA replication, NHEJ repair has been proposed to be deleterious due to the intrinsic increased incidence of breaks, especially one ended DSBs, whose inappropriate joining could lead to dicentric chromosomes that initiate break-fusion cycles and complex chromosome rearrangements (Gaillard et al., 2015; Gelot et al., 2015). Therefore, NHEJ-mediated mutagenic repair is believed to be a major contributor to genomic instabilities and tumorigenesis that arise when the HR machinery is defective (Deng and Wang, 2003; Prakash et al., 2015). The ability of cells to inhibit NHEJ and promote error-free HR repair during DNA replication is essential for genome integrity.

A critical step in regulating the choice of HR or NHEJ for repair is the control of 5'-to-3' nucleolytic processing of DNA ends (also known as resection), as the formation of long 3' ssDNA tails naturally promotes HR while preventing NHEJ (for review see (Chapman et al., 2012b; Prakash et al., 2015)). 53BP1 is a scaffolding protein that plays a major role in limiting resection (Bothmer et al., 2010; Bunting et al., 2010). Although the mechanism by which 53BP1 limits resection remains incompletely understood, it involves the 53BP1-dependent recruitment of the additional anti-resection factors such as RIF1 (Callen et al., 2013; Chapman et al., 2013; Di Virgilio et al., 2013; Escribano-

Diaz et al., 2013; Kumar and Cheok, 2014; Zimmermann et al., 2013). On the other hand, in S-phase, the tumor suppressor BRCA1 is proposed to play a pro-HR function by counteracting the recruitment of 53BP1 to DSBs, therefore enabling resection (Bunting et al., 2010). This model is supported by genetic data in mice showing that the loss of 53BP1 suppresses embryonic lethality, genomic rearrangements and tumorigenesis seen in mice lacking functional BRCA1 (Bouwman et al., 2010; Bunting et al., 2010; Cao et al., 2009; Prakash et al., 2015). DNA end resection is inhibited during S-phase in cells lacking BRCA1, and the increased recruitment of 53BP1 to replication-induced lesions results in increased chromosomal aberrations, which has been suggested to occur through mutagenic NHEJ repair (Bunting et al., 2010; Escribano-Diaz et al., 2013). Collectively, these observations support a model for repair pathway choice in which BRCA1 and 53BP1 compete for the sites of DNA lesions to promote HR or NHEJ. Despite strong genetic evidence supporting this model, it remains unclear exactly how 53BP1 promotes chromosomal instabilities upon BRCA1 dysfunction, as NHEJ is not the only potential source of mutagenic repair. For example, de-regulated HR also has the potential to result in genomic instabilities, such as gross chromosomal rearrangements, due to recombination between non-allelic sequences (Carr and Lambert, 2013; Kolodner et al., 2002). The role of BRCA1 in suppressing genomic instability during DNA replication may be dependent not only on counteracting 53BP1-mediated NHEJ, but also on ensuring that HR is properly executed for error-free repair. While several mechanisms have been proposed to explain how the competition between BRCA1 and 53BP1 for DNA lesions is regulated (Kakarougkas et al., 2013; Orthwein et al., 2015; Tang et al., 2013; Zhang et al., 2016), the molecular mechanism by which BRCA1 is able to efficiently counteract 53BP1 during replication stress to favor DNA end resection remains incompletely understood.

While many aspects of mammalian DNA repair are conserved in budding yeast, it remains unknown whether key mechanisms of HR-control and DNA repair pathway choice are also conserved. Notably, a clear sequence homolog or a functional analog of BRCA1 has not been identified in fungi. On the other hand, the 53BP1 ortholog Rad9 has been shown to play a conserved role in blocking resection (Clerici et al., 2014; Ferrari et al., 2015; Lazzaro et al., 2008). Cells lacking *RAD9* resect DSBs faster and more extensively (Chen et al., 2012; Clerici et al., 2014; Lazzaro et al., 2008). Of importance, it was recently proposed that a complex formed by the DNA repair scaffolds Slx4 and Rtt107 is able to counteract the engagement of Rad9 at replication-induced lesions to dampen DNA damage checkpoint signaling (Ohouo et al., 2013). Given the roles of Rad9 in blocking resection, we predicted that the ability of Slx4-Rtt107 to counteract Rad9 recruitment to DNA lesions would help avert the block, therefore promoting resection. Indeed, recent work presented experimental evidence that the Slx4-Rtt107 complex favors resection of DSBs (Dibitetto et al., 2016).

Mammalian TOPBP1^{Dpb11} is an essential scaffolding protein that plays evolutionarily conserved roles in initiation of DNA replication and activation of DNA damage checkpoint signaling (Boos et al., 2011; Navadgi-Patil and Burgers, 2008; Pfander and Diffley, 2011; Puddu et al., 2008; Tanaka et al., 2007; Zegerman and Diffley, 2007). TOPBP1^{Dpb11} is comprised of multiple BRCT (BRCA1 C-terminus) domains (9 in humans and 4 in yeast), which are protein interacting modules that often recognize phosphorylated motifs (Manke et al., 2003; Rodriguez et al., 2003; Yu et al., 2003). TOPBP1^{Dpb11} recognizes phospho-proteins to assemble multi-subunit complexes required for replication initiation or checkpoint activation (Boos et al., 2011; Pfander and Diffley, 2011; Tak et al., 2006; Zegerman and Diffley, 2007). Although TOPBP1 has been implicated in HR repair (Germann et al., 2011; Liu and Smolka, 2016; Morishima et

al., 2007; Moudry et al., 2016), its precise role and mode of action remain largely elusive. Here we show that in budding yeast, Dpb11 plays a decisive role in the control of DNA end resection, the first key step in HR, by mediating a competition between the anti-resection protein Rad9 and the pro-resection scaffolds Slx4-Rtt107 for DNA lesions. In humans, we find that TOPBP1 coordinates the recruitment of 53BP1 via a physical interaction that appears to be mutually exclusive with that of the pro-HR factor BRCA1. Our results support a model in which TOPBP1^{Dpb11} controls the mutually exclusive engagement of antagonistic regulators of recombinational DNA repair for the proper maintenance of genome integrity.

Results

BRCT domains of Dpb11 mediate mutually antagonistic functions in DNA end resection

In budding yeast, Dpb11 has been shown to recruit Rad9 to the 9-1-1 clamp loaded at DNA lesions to promote activation of the DNA damage checkpoint (Fig. 1A) (Abreu et al., 2013; Granata et al., 2010; Pfander and Diffley, 2011; Wang et al., 2012). Since Rad9 and its human ortholog 53BP1 have both been shown to block DNA end resection, we hypothesized that the role of Dpb11 in mediating the recruitment of Rad9 to DNA breaks plays a decisive role in resection control and HR-mediated DNA repair. To test this, we fused BRCT domains 3/4 of Dpb11 with full-length Rad9 (Fig. 1B), with the expectation that this chimera would hyper-stabilize Rad9 at DNA lesions and block resection. Using a system to induce a persistent DSB at the MAT locus through the over-expression of HO endonuclease (Lee et al., 1998; White and Haber, 1990) we found that the Dpb11$^{BRCT3/4}$-Rad9 chimera (hereinafter referred to as 'B3/4-Rad9') is robustly detected at 0.15 kb from the break site using ChIP-qPCR (Fig. 1C). Of importance, a point mutation corresponding to K544A in Dpb11, known to disrupt the ability of BRCT-3/4 to recognize phosphorylated 9-1-1, prevents the stabilization of B3/4-Rad9 near the site of DSB (Fig. 1C). Taking advantage of this system, we assessed the effect of Dpb11-mediated Rad9 hyper-stabilization on resected DNA ends using an assay to monitor the accumulation of ssDNA flanking an irreparable HO-induced DSB site (Dibitetto et al., 2016; Ferrari et al., 2015). Although we did not observe an impact on resection at 0.15 kb from the break, resection is significantly inhibited at 1.4 kb and severely blocked at 4.8 kb from the break site upon expression of the B3/4-Rad9 chimera (Fig. 1D). The K544A mutation that impairs BRCT-3/4 fully restored resection, arguing that the ability of

Dpb11 to bridge Rad9 to the 9-1-1 complex is crucial to inhibit long-range resection. Consistent with this model, expression of the B3/4-Rad9 chimera strongly impaired the repair of one HO cut through a single strand annealing (SSA) mechanism that relies on extensive resection (Figs. 1E-G).

We have recently proposed a model in which Dpb11 also coordinates the controlled disengagement of Rad9 from lesions for dampening checkpoint signaling (Fig. 1H) (Cussiol et al., 2015; Ohouo et al., 2013). In this model, the Slx4-Rtt107 scaffolding complex competes with Rad9 for Dpb11 interaction, ultimately preventing Rad9 from stabilizing at DNA lesions. We hypothesized that this competition mechanism is also crucial to control the roles of Rad9 in DNA repair and could provide the molecular basis to understand how 53BP1 recruitment is regulated in mammals. We predicted that a fusion of the Slx4-Rtt107 complex with Dpb11 BRCT-3/4 should be able to antagonize the B3/4-Rad9 chimera and restore resection. We have previously shown that a fusion of Dpb11 BRCT3/4 with Rtt107 BRCT-5/6 (referred as MBD: minimal multi-BRCT domain module) (Fig. 1I) mimics the role of the Dpb11-Slx4-Rtt107 complex in checkpoint dampening (Cussiol et al., 2015). Here we found that expression of MBD prevents hyper-stabilization of the B3/4-Rad9 chimera at DSBs (Fig. 1J) and, strikingly, fully suppresses the resection block induced by B3/4-Rad9 (Fig. 1K). Collectively, the above results are consistent with a model in which Dpb11 plays mutually antagonistic roles in resection by coordinating the stabilization as well as exclusion of Rad9 from DNA lesions (Fig. 1H and L).

Dpb11-mediated recruitment of Rad9 impairs HR-mediated repair in response to replication stress

Slx4 and Rtt107 have been shown to be particularly important in the response to methyl

methanesulfonate (MMS)-induced replication stress (Chin et al., 2006; Fricke and Brill, 2003; Ohouo et al., 2010; Roberts et al., 2006). We therefore asked whether the B3/4-Rad9 chimera also impairs the control of resection and HR-mediated repair in cells treated with MMS, a DNA alkylating agent that blocks replication fork progression. While MMS treatment resulted in the formation of multiple RPA foci, an indirect marker of ssDNA exposure, in cells expressing the mutated BRCT-3/4(K544A)-Rad9 chimera, expression of the chimera B3/4-Rad9 bearing functional BRCT-3/4 prevented most cells from accumulating multiple RPA foci (Fig. 2A-B), consistent with the less accumulation of ssDNA at replication forks likely due to inhibition of DNA end resection. This defect in RPA foci formation is accompanied by a severe reduction in foci formation of the HR protein Rad52 (Fig. 2C-D), pointing to an impairment of HR-mediated repair. Of note, co-expression of the MBD chimera restored the accumulation of RPA and Rad52 foci in cells expressing B3/4-Rad9 chimera. These results support that Dpb11-mediated recruitment of Rad9 also plays an important role in coordinating DNA end resection and HR repair in the response to replication blocks. MBD co-expression or the K544A mutation in the B3/4-Rad9 chimera were also sufficient to rescue B3/4-Rad9-induced MMS sensitivity (Fig. 2E and F). Furthermore, expression of B3/4-Rad9 led to hyper-activation of the checkpoint effector kinase Rad53 in cells treated with MMS as evaluated by the mobility shift of Rad53 (Fig. 2G), consistent with the Dpb11-mediated function of Rad9 in promoting checkpoint signaling. This aberrant Rad53 hyper-phosphorylation as well as the appearance of a hyper-shifted form of B3/4-Rad9 was suppressed by the co-expression of MBD, which is in agreement with the reduced binding of B3/4-Rad9 nearby an HO-induced DSB upon MBD expression. These data again reinforce the competition-based model in which Dpb11 regulates HR-mediated repair by coordinating the mutually exclusive recruitment of Slx4 and Rad9, and reveal that Dpb11 plays antagonistic roles in HR-mediated repair also in the context of

replication stress.

The Mec1 kinase promotes resection via phosphorylation of Slx4

According to our model, the control of Dpb11 interactions with Slx4 or Rad9 is expected to play a key role in the control of DNA end resection. Therefore, the decision to specifically stabilize the Dpb11-Slx4 interaction should be the distinguishing molecular event that transitions Dpb11's function from blocking resection to favoring resection. Since interactions of Dpb11 with Slx4 and Rad9 are both dependent on CDK (Gritenaite et al., 2014; Ohouo et al., 2013; Pfander and Diffley, 2011; Wang et al., 2012), we reasoned that CDK activity is unlikely to be the discerning molecular event that commands the choice of Slx4 versus Rad9 stabilization at DNA lesions. Previously, we have shown that the Dpb11-Slx4 interaction is strongly induced by DNA damage and requires the Mec1 kinase (Ohouo et al., 2010). Here we show that Mec1 is specifically required to enhance the Dpb11-Slx4 interaction, but plays a minor role in the control of the Dpb11-Rad9 interaction (Figs. 3A and B). During MMS-induced replication stress or phleomycin-induced DSBs in G2/M, the Slx4-Dpb11 interaction was largely dependent on Mec1. On the other hand, we observed only a slight reduction of the Rad9-Dpb11 interaction upon deletion of *MEC1*. These results are consistent with the model in which Mec1 signaling plays a decisive role in promoting DNA end resection via Slx4 phosphorylation. To test this, we analyzed resection in the *slx4-7MUT* mutant bearing mutation of 7 Mec1-consensus phosphorylation sites, which we have previously shown to specifically impair binding to Dpb11, but not to impair binding to other Slx4-interacting proteins (Ohouo et al., 2010; Ohouo et al., 2013). As shown in Fig. 3C, resection in the *slx4-7MUT* mutant was impaired, close to the level observed in cells lacking *SLX4*. We therefore propose a model in which Mec1 signaling, through the formation of a Dpb11-Slx4-Rtt107 complex, counteracts a resection block imposed by the Rad9-Dpb11

complex (Fig. 3D).

Proteomic analysis in human cells reveals TOPBP1 interactions with antagonistic repair factors

Based on our findings in yeast, we speculated that TOPBP1 also plays a role in coordinating the recruitment of antagonistic factors for the proper control of DNA repair in mammals. Previous reports revealed that TOPBP1 indeed interacts with 53BP1 as well as with a range of pro-HR factors, including BRCA1-associated proteins (Cescutti et al., 2010; Greenberg et al., 2006; Morishima et al., 2007; Yamane et al., 2002; Yoo et al., 2009). We reasoned that TOPBP1 interactions specifically induced by replication stress should reveal pro-HR functions for TOPBP1. We therefore performed an unbiased mass spectrometry analysis to define the network of TOPBP1 interactions in cells either treated with hydroxyurea (HU) to induce replication stress, or with nocodazole to reveal interactions that are independent of replication stress (Fig. 4A). Next, we measured the changes of the identified interactions by directly comparing cells treated with HU or nocodazole in order to specifically reveal interactions induced by replication stress (Fig. 4B). While most interactions did not display major changes in our comparison (Fig. 4B), the interaction of human TOPBP1 with a pro-HR factor, BRCA1, is strongly induced by replication stress (Fig. 4B), similar to what we previously observed for yeast Dpb11 (Ohouo et al., 2010). Of interest, the interaction of TOPBP1 with 53BP1 is reduced under replication stress (Figs. 4B-C), suggesting that the interactions of TOPBP1 with BRCA1 and 53BP1 are mutually exclusive. Similar results were observed when comparing untreated asynchronous cells with HU-treated cells (Fig. S1C), further suggesting that the TOPBP1-53BP1 interaction is largely constitutive, and is counteracted upon replication stress. This notion is further supported by the findings that both of these interactions are disrupted by mutations that impair BRCT-1/2 or BRCT-4/5

domains of TOPBP1 (Fig. 4D), and that BRCA1 could not be detected in a 53BP1 immunoprecipitation, and vice-versa (Figs. S1A-B). Because 53BP1 and BRCA1 localize to sites of DNA lesions in a mutually exclusive manner (Chapman et al., 2012a), and have been proposed to compete for DNA lesions to dictate repair pathway choice (Bouwman et al., 2010; Bunting et al., 2010; Cao et al., 2009; Chapman et al., 2012a), our findings suggest that TOPBP1 could be the mediator of such competition, similar to the role of Dpb11 in coordinating the competition between Rad9 and Slx4 in yeast. Also similar to the yeast model, the ATR kinase plays an important role in promoting the interaction of TOPBP1 with a pro-HR factor, in this case BRCA1, but is not required for enhancing the TOPBP1-53BP1 interaction (Fig. 4E). Overall, these findings are consistent with a model in which yeast Dpb11 and mammalian TOPBP1 have roles in coordinating the action of antagonistic repair factors (Fig. 4F).

Hyper-stabilization of the TOPBP1-53BP1 interaction promotes 53BP1 recruitment to nuclear foci in S-phase

Based on our findings in yeast, we hypothesized that human TOPBP1 controls the recruitment of 53BP1 to DNA lesions under certain conditions and is important to mediate 53BP1-dependent DNA repair. To test this hypothesis, we engineered a system to stabilize the 53BP1-TOPBP1 interaction. We were unable to generate a chimeric mammalian protein similar to the B3/4-Rad9 fusion we generated in yeast, since fusion proteins of 53BP1 with BRCT domains of TOPBP1 did not express in human cells lines. To circumvent this issue, we fused 53BP1 to a 120 amino acid region from the N-terminal domain of RFC1 (replication factor C subunit 1), which we found to constitutively interact with TOPBP1 (Fig. 4B). Thus, by fusing the N-terminus of RFC1 (hereinafter referred to as Constitutive TOPBP1-interacting Region, CTR) to 53BP1 (Fig. 5A), we reasoned that the interaction of this chimera with TOPBP1 would be stabilized

and enhanced during replication stress. Indeed, the CTR-53BP1 chimeric protein displays enhanced interaction with TOPBP1 after hydroxyurea (HU) treatment (Fig. 5B). Strikingly, the CTR-53BP1 chimera forms significantly more nuclear foci compared to 53BP1 alone in cells progressing through S-phase following release from an HU-induced arrest (Figs. 5C-D and Fig. S2A), suggesting the enhanced recruitment of CTR-53BP1 to replication-induced lesions.

Once recruited to the lesion site, 53BP1 promotes the recruitment of PTIP and RIF1, two proteins believed to function as effectors of NHEJ and/or blockers of resection (Callen et al., 2013; Chapman et al., 2013; Di Virgilio et al., 2013; Escribano-Diaz et al., 2013; Feng et al., 2013; Zimmermann et al., 2013). To investigate whether the increased recruitment of CTR-53BP1 functionally impacts 53BP1-mediated DNA repair, we first monitored PTIP and RIF1 status. Interestingly, CTR-53BP1 pulled down more PTIP compared to 53BP1 alone, despite the relatively lower expression level of CTR-53BP1 (Fig. 5B). In addition, while we were unable to monitor PTIP foci using available antibodies, we found that CTR-53BP1 induces a significant increase in the number of RIF1 foci in S-phase cells released from a HU arrest (Figs. 5C-D and Fig. S2A). Since RIF1 and PTIP recruitment to DNA lesions is believed to require DNA damage-induced phosphorylation of 53BP1 (Callen et al., 2013; Chapman et al., 2013; Di Virgilio et al., 2013; Escribano-Diaz et al., 2013; Kumar and Cheok, 2014; Munoz et al., 2007; Zimmermann et al., 2013), our results strongly suggest that the enhanced interaction with TOPBP1 increases the engagement of CTR-53BP1 at sites of lesions, culminating in its phosphorylation and subsequent increased recruitment of RIF1, and likely PTIP.

Hyper-stabilization of the TOPBP1-53BP1 interaction impairs HR-mediated repair and induces chromosomal aberrations

The foci formed by CTR-53BP1 co-localized with γ-H2AX and RIF1 but not with RPA or RAD51, two markers for HR (Fig. S2B), suggesting that the chimera is engaging in RIF1-mediated DNA repair in a mutually exclusive manner with the HR-machinery. We therefore hypothesized that expression of CTR-53BP1 would induce genomic instability by promoting mutagenic NHEJ repair and/or deregulating HR-mediated repair. Indeed, we observed a significant increase in the number of chromosomal aberrations induced by the expression of CTR-53BP1, but not by the expression of ectopic 53BP1, in response to fork collapse induced by a combination of PARP inhibitor (AZD2461) and ATR inhibitor (VE-821) (Fig. 5E). We have also generated HEK293T cells with a stably integrated CTR-53BP1 whose expression is induced by doxycycline (DOX) (Fig. 5F and Fig. S3A-B). In these cells, DOX treatment led to growth sensitivity (Fig. S3C) and a striking accumulation of chromosomal aberrations, especially radial chromosomes, upon PARP inhibition (Figs. 5G-H). We could observe some radials in these cells even in the absence of DOX (Fig. 5H), which we attribute to a minor leakage expression of CTR-53BP1 in the absence of DOX (Fig. S3A). Of importance, we note that overexpression of 53BP1 has only minor impact in the cells we have used. Despite ectopic 53BP1 being expressed at least 5 times more than CTR-53BP1 (Fig. 5B and Fig. S4B), overexpression of 53BP1 did not result in significant increase in chromosomal aberrations (Fig. 5E). Collectively, these findings support a model in which TOPBP1 mediates the recruitment of 53BP1 to DNA lesions to promote 53BP1-dependent genomic instability.

Consistent with the model that the 53BP1-TOPBP1 interaction counteracts HR-mediated DNA repair, we observed that expression of CTR-53BP1 reduced HR repair in the DR-GFP system (Fig. 5I), a commonly used assay to test HR in human cells (Gunn and Stark, 2012). Again, overexpression of 53BP1 had only a minor effect in inhibiting HR

(Figs. S4A-B), further consistent with the model that interaction of 53BP1 with TOPBP1 is important to stabilize 53BP1 at DNA lesions and counteract HR-mediated repair. Expression of CTR-53BP1 bearing mutations in the tudor or UDR domains, which are important for the ability of 53BP1 to localize to sites of DNA lesions, also failed to reduce HR-repair in the DR-GFP system (Figs. S4A-B), supporting that the ability of CTR-53BP1 to counteract HR requires recruitment to chromatin as well as TOPBP1 binding. As we observed in yeast, our results suggest that this effect is associated with a 53BP1-mediated block in DNA end resection. Although assays to measure DNA end resection in mammalian cells are not as well established as in yeast, we were able to observe a significant reduction in SSA repair (Fig. 5J) through an assay that relies on extensive resection (Gunn and Stark, 2012), and a mild, but consistent, reduction in DNA end resection next to a DSB break that was induced through the ER-*Asi*SI system (Fig. 5K and Fig. S4C) (Iacovoni et al., 2010; Zhou et al., 2014). Finally, we noticed that the ability of CTR-53BP1 to induce chromosomal aberrations and impair HR-mediated repair was stronger upon siRNA-mediated knock-down of BRCA1 (Figs. 5L-M and Figs.,S5A-B). Congruent with the idea that the anti-HR function of the TOPBP1-53BP1 interaction is being counteracted by BRCA1, a partial reduction in BRCA1 abundance (see Fig. S5B) strongly induced chromosomal aberrations upon CTR-53BP1 expression. Overall, while further investigation will be necessary to understand how TOPBP1 controls recombinational DNA repair and repair pathway choice, the results presented here are consistent with a model in which TOPBP1 mediates the competition between 53BP1 and BRCA1 for DNA lesions. As shown in Fig. 5N, we propose a working model where the ability of TOPBP1 to bind to 53BP1 is important to stabilize 53BP1 at DNA lesions. In cells lacking functional BRCA1, TOPBP1 would promote 53BP1-mediated genomic instability possibly by blocking resection, impairing error-free HR-mediated repair and promoting mutagenic NHEJ repair. In normal cells, ATR would play a role in preventing

genomic instability by promoting the BRCA1-TOPBP1 interaction and counteracting the engagement of 53BP1 at DNA lesions.

Discussion

Maintenance of genome integrity during DNA replication heavily relies on HR-mediated DNA repair. In *BRCA1* mutated cells lacking a functional HR machinery, the scaffolding protein 53BP1 plays a key role in promoting replication stress-induced chromosomal aberrations. In the last 10 years, the discovery that BRCA1 and 53BP1 play antagonistic roles in the control of DNA end resection provided a mechanistic explanation for how lack of BRCA1 results in 53BP1-mediated genomic instability. However, it remains incompletely understood how the engagement of BRCA1 and 53BP1 at DNA lesions is regulated, and which molecular mechanisms govern a likely competition between these factors. Here we build on mechanistic work in yeast to propose a central and evolutionarily conserved role for the TOPBP1/Dpb11 scaffold in controlling the engagement of pro and anti-resection factors for DNA repair control. We provide evidence to support that interactions of Dpb11 with the Rad9 and Slx4-Rtt107 scaffolds define a key phospho-regulated molecular circuitry for resection control. We also provide initial evidence to support a model in which mammalian TOPBP1 mediates a similar system for DNA repair control via the coordinated engagement of 53BP1 and BRCA1.

Central to this circuitry for resection control is the ability of Dpb11/TOPBP1 to function both as a scaffold as well as an activator of Mec1/ATR, therefore integrating the action of this kinase into resection control. In our proposed model depicted in Fig. 3D for yeast, Dpb11 functions as a scaffolding module to stabilize pro- or anti-resection factors at DNA lesions, and activation of the Mec1 kinase plays a decisive role in shifting Dpb11's role from an inhibitor of resection (via the Dpb11-Rad9 complex) to a positive regulator

of resection (via the Dpb11-Slx4-Rtt107 complex). Interestingly, when bound to Rad9, Dpb11 is also coordinating Mec1 signaling, but in this case, it is contributing to transduce Mec1 signaling towards Rad53 activation (Pfander and Diffley, 2011; Puddu et al., 2008). Notably, Rad53 signaling contributes to inhibit DNA end resection by inhibiting the action of the Exo1 nuclease (Morin et al., 2008; Segurado and Diffley, 2008). Therefore, the Mec1-dependent shift in Dpb11 interaction from Rad9 to Slx4 is a key event in this circuitry, resulting in a drastically different output in resection control. It is tempting to speculate that early in the response to DNA lesions, the Dpb11-Rad9 complex activates the checkpoint to promote, among other outputs, a protection for replication forks and DSB ends from detrimental and unregulated resection. With the subsequent build up in Mec1 signaling at these sites, coordinated HR-mediated repair is evoked by phosphorylation of Slx4, which promotes the Slx4-Dpb11 interaction, destabilizes Rad9 engagement at DNA lesions and therefore favors resection. Consistent with this model, our results using fusion proteins recapitulate the importance of Dpb11 for the stabilization of Rad9 at DNA lesions and show that a simple multi-BRCT domain (MBD) module competing for binding to the 9-1-1 complex and phospho-H2A can completely counteract the engagement of Rad9 and strongly promote resection.

In human cells we propose that, similar to the Dpb11-mediated circuitry, TOPBP1 also mediates a phospho-regulated circuitry for HR control. Our results are consistent with a model in which the BRCA1-TOPBP1 interaction plays a role analogous to the Dpb11-Slx4 interaction in yeast to prevent TOPBP1-mediated stabilization of 53BP1 at DNA lesions. Interestingly, the mammalian circuitry seems to follow a similar regulatory logic we observed in the yeast system. While TOPBP1 interacts with both BRCA1 and 53BP1, the ATR kinase specifically promotes the TOPBP1-BRCA1 interaction, but not the

TOPBP1-53BP1 interaction. We speculate that the ATR-mediated TOPBP1-BRCA1 interaction functions similar to the Dpb11-Slx4 interaction, counteracting the TOPBP1-53BP1 interaction and destabilizing the engagement of 53BP1 at DNA lesions. We note that human SLX4 was also identified as a TOPBP1 interactor, consistent with a previous report (Gritenaite et al., 2014). However, the interaction of TOPBP1 with SLX4 is not enhanced by replication stress, suggesting a fundamentally distinct mode of interaction compared to the Dpb11-Slx4 interaction in yeast.

Much remains unclear about the mechanism and regulation of TOPBP1 interactions with BRCA1 and 53BP1. Dissecting the mechanism of these interactions will be essential to better understand how TOPBP1 and ATR control resection, and how TOPBP1 helps promote 53BP1-mediated repair. Regulation of the TOPBP1-BRCA1 seems more complex than regulation of the Dpb11-Slx4 interaction in yeast as it has been previously shown that ATM and DNA-PK can also promote the TOPBP1-BRCA1 interaction (Greenberg et al., 2006). Since those experiments were performed in response to ionizing radiation (IR), further work is necessary to precisely define the role of each kinase under distinct forms of DNA damage. Nonetheless, our results support that ATR plays a more prominent role during replication stress in mediating the TOPBP1-BRCA1 interaction as compared to ATM and DNA-PK. This is congruent with the idea that ATR is a key inducer of HR-mediated repair during replication stress. Generation of separation-of-function *BRCA1* mutants bearing mutations in phosphorylation sites that mediate interaction with TOPBP1 will be required to further determine the precise extent to which ATR-mediated HR depends on the TOPBP1-BRCA1 interaction. We envision that ATR-dependent formation of the BRCA1-TOPBP1 interaction is likely one of the key events required for ATR-mediated resection. As such, understanding the TOPBP1-

mediated circuitry for phospho-regulation of resection could have implications for understanding how to best use ATR inhibitors in cancer therapy.

It has been recently reported that depletion of TOPBP1 abrogates RAD51 loading to chromatin and formation of RAD51 foci, but does not impair DNA end resection or RPA loading (Moudry et al., 2016). Based on our model, we predict that in Moudry *et al.*'s experimental setup the absence of TOPBP1 would also impair 53BP1-mediated resection block, thereby allowing productive DNA end processing to occur. In fact, the scenario would be similar to what is observed in cells lacking both BRCA1 and 53BP1, where resection is restored as compared to cells lacking only BRCA1 (Bunting et al., 2010). Therefore, the findings by Moudry *et al*. are fully consistent with our model that TOPBP1 is important to promote 53BP1 functions in DNA repair. Consistent with this model, stabilization of the 53BP1-TOPBP1 interaction reduced the efficiency of HR-mediated repair and resection. We acknowledge that our method for monitoring resection is not yet set to measure resection of distances farther from the break, and that the effect of blocking long-range resection at distances over 2 kb from the break may be stronger, as we observed for yeast. The mild effect in resection may also be related to the expression level of the CTR-53BP1 fusion, which was not dramatically higher than expression level of endogenous 53BP1 (Fig. S3B). In the future it will be interesting to measure resection in mutants where the 53BP1-TOPBP1 interaction is disrupted, and determine whether these mutants may restore HR-mediated repair in BRCA1-deficient cells. Along these lines, it will be important to define how 53BP1 (and the 53BP1-TOPBP1 interaction) promotes chromosomal abnormalities upon BRCA1 deficiency. While these abnormalities have been proposed to be driven by 53BP1-mediated NHEJ, it is conceivable that genomic instability may arise through deregulated and error-prone

HR-mediated repair, as the action of 53BP1 in negatively regulating resection may not completely block resection, but result in aberrantly regulated resection. Overall, our findings presented here provide important insights into the mode of action of TOPBP1^{Dpb11} in the control of DNA repair and should have implications for understanding how genomic instabilities and cancer arise in individuals with a defective HR-machinery.

Acknowledgements

This work was supported by grants to M.B.S. from the National Institutes of Health (R01-GM097272), to R.W. from the National Institutes of Health (R01-CA108773), to A.P from Associazione Italiana per la Ricerca sul Cancro (AIRC IG-15488) and CARIPLO (2013-0790) and to R.F. from the Spanish Ministry of Economy and Competitiveness (SAF2013-49149-R, BFU2014-51672-REDC) and Fundacion CajaCanarias (AP2015/008). J.R.S. was supported by training grant T32GM007273 from the National Institutes of Health. We thank the members of all labs involved for comments and suggestions.

Materials and Methods

Yeast strains, plasmids, media and growth conditions.

Strains generated in this study were derived from S288C or JKM139. HA and FLAG tags were inserted by homologous recombination at specific genomic loci (all proteins were tagged at the C-terminus and the expression was verified by western blot). Tagged strains were assayed for sensitivity to MMS to ensure they displayed similar sensitivity as wild-type strains. Standard cloning methods were used to generate the plasmids for this study. The *B3/4-RAD9* chimera was generated using a stitch PCR protocol. Briefly, we fused the *RAD9* promoter (450 base pairs upstream of the start codon) to the BRCT3/4 of *DPB11* (corresponding to amino acids 292-600 of Dpb11) and the resulting PCR product was stitched to the *RAD9-3xFLAG* sequence (see Fig. 1B for the schematic illustration of the resulting chimeric protein). The final PCR product was subsequently cloned into *pRS416* (for ectopic expression) or *pFA6A* (for integration at the endogenous *RAD9* locus). All point mutations were generated by site-directed mutagenesis using the Primestar® Max DNA Polymerase (Takara). The plasmid for expression of the MBD fusion protein was constructed as previously reported (Cussiol et al., 2015). All yeast strains and plasmids used in this study are described in Supplementary Tables S1 and S2, respectively. Yeast cells expressing genes with the indicated epitope tags were cultured in YPD or in synthetic complete medium lacking uracil and/or tryptophan when carrying an expression plasmid with *URA3* or *TRP1* (derivatives from *pRS416* and *pRS414*, respectively). Cells were grown to log phase, subjected to MMS treatment as specified in the figures and collected by centrifugation. For the experiments using the JKM139 and YMV80 strains, cells were grown in YP medium enriched with 2 % glucose (YPD), 3 % raffinose (YP raff) or 3 % raffinose and

2 % galactose (YP raff gal). All the synchronization experiments were performed at 28^{o}C.

ChIP analysis in yeast

ChIP analysis for detection of proteins nearby an HO cut site was performed in nocodazole-arrested cells as described previously (Ferrari et al., 2015). The oligonucleotides used are listed in Table S6. Data are presented as fold enrichment at the HO cut site (0.15 kb from DSB) over that at the *PRE1* locus on chromosome V and then normalized by the corresponding input sample.

Co-immunoprecipitation procedure in yeast

Co-immunoprecipitation experiments for yeast lysates were performed as described previously (Cussiol et al., 2015).

Mammalian cell culture

Human U2OS, HEK293T and HEK293 Flp-In T-REx cell lines were grown in DMEM media supplemented with 10% BCS, non-essential amino acid and penicillin/streptomycin (Corning). The HEK293 Flp-In T-REx cell line for expression of doxycycline-inducible FLAG-CTR-53BP1, and a control cell line, were generated by stable transfection using the Flp-In T-REx system (Thermo Fisher Scientific Cat# R78007) according to manufacture instructions and were cultured in 10% BCS/DMEM media supplemented with 50ug/ml hygromycin B. To induce protein expression in HEK293 Flp-In T-REx cell lines, 2 μg/ml doxycycline was added to the culture media for 48 h. Plasmid transfections were generally carried out using homemade PEI (Polysciences, Inc.), jetPRIME PEI (Polyplus) or Lipofectamine 2000 (Thermo Fisher Scientific). siRNA transfection were performed using Lipofectamine RNAiMax (Thermo Fisher Scientific). In general, cells were subjected to the indicated drug treatment 48 h

post-transfection and then fixed or harvested for microscopy and immunoprecipitation experiments. Specifically, for immunoprecipitation experiments, HEK293T cells were treated for either 24 h with HU (1 mM) or 14 h with nocodazole (100 ng/mL) 48 h post-transfection before harvesting. For the ATR inhibition experiments (Fig. 4E), cells were pre-treated with the indicated inhibitors (10 μM ATR inhibitor (VE-821), 10 μM ATM inhibitor (KU-55933), 5 μM DNA-PK inhibitor (NU7441)) for 45 min before the additional treatment with 2.5 mM HU for another 30 min in the presence of the according inhibitors.

Co-immunoprecipitation procedures in mammalian cells

For co-immunoprecipitation experiments, cell pellets were lysed for 30 min on ice in modified RIPA buffer (50 mM Tris-HCl pH 7.5, 150 mM NaCl, 1% tergitol, 0.25% sodioum deoxycholate, 5mM EDTA) supplemented with Complete EDTA-free protease inhibitor cocktail (Roche), 5 mM sodium fluoride, 10 mM β-glycerol-phosphate, 1 mM PMSF and 0.4 mM sodium orthovanadate. Protein lysates were cleared by 10 min centrifugation to pellet cell debris and then incubated with anti-TOPBP1 resin, anti-HA or FLAG agarose beads (Sigma-Aldrich) for 4 h at 4°C. Immunoprecipitates were then washed three times with the modified RIPA buffer and then eluted using 3 resin volumes of the elution buffer (0.5 μg/mL of FLAG peptide in 50 mM Tris-HCl and 0.2 % tergitol for anti-FLAG resin; 100 mM Tris-HCl pH 8.0 and 1 % SDS for others).

Immunoblotting analysis

Whole cell lysates and eluents were denatured with 3X SDS sample buffer (composed of bromophenol blue, stacking gel buffer, 50 % glycerol, 3 % SDS and 60 mM DTT) and resolved on SDS-PAGE gels. Proteins were then transferred onto polyvinylidene fluoride (PVDF) membranes and probed with desired antibodies.

Mass spectrometry analysis

For mammalian SILAC experiments, HEK293T cells were grown in SILAC DMEM media lacking arginine and lysine (ThermoFisher Scientific 88425) supplemented with 10 % dialyzed FBS and penicillin/streptomycin. “Light” DMEM media were supplemented with “light” (normal) arginine and lysine; ‘‘heavy’’ DMEM media were supplemented with “heavy” lysine $^{13}C6$, $^{15}N2$ and “heavy” arginine $^{13}C6$, $^{15}N4$. Cells were treated with 1 mM HU for 24 h or 100 ng/ml nocodazole for 14 h before harvesting. TOPBP1 was immunoprecipitated using affinity-purified TOPBP1 antibodies or antibodies that recognize the according epitope tags. Immuno-precipitated proteins were then reduced, alkylated, precipitated and digested by trypsin. The peptides were desalted, dried, reconstituted in 80 % acetonitrile and 1 % formic acid and then fractionated by Hydrophilic Interaction Chromatography (HILIC). Fractions were dried, reconstituted in 0.1 % trifluoroacetic acid, and analyzed by LC-MS/MS using a Q-Exactive Orbitrap mass spectrometer as previously described (Bastos de Oliveira et al., 2015). Database search and quantitation of heavy/light peptide isotope ratios were performed as previously described (Bastos de Oliveira et al., 2015).

Chemicals and antibodies

PARP inhibitor (AZD2461), ATM inhibitor (KU-55933), DNA-PK inhibitor (NU7441) and ATR inhibitor (VE-821) were purchased from Selleckchem. Nocodazole was purchased from Calbiochem. Hydroxyurea and MMS were purchased from Acros Organics. Antibodies used for detection of yeast proteins were the following: anti-Rad53 antibody (clone Mab EL7, 1:30 dilution); anti-FLAG (M2 F1804; Sigma, 1:5000 dilution), anti-HA (12CA5; Roche, 1:10000 dilution), ECL HRP-linked secondary antibody (NA931-GE, 1:10000 dilution). The following antibodies were used for the detection of proteins in human cells: anti-FLAG (M2, F1804; Sigma), anti-HA.11 (MMS-101P; Covance), 53BP1

(NB100-304; Novus Biologicals), RIF1 (sc-55979; Santa Cruz), phospho-KAP-1(S824) (A300-767A-T; Bethyl) phospho-CHK1 (Ser345) (#2341; Cell Signaling), BRCA1(#OP92, MS110; Calbiochem). TOPBP1 and BRCA1 antibodies were previously described (Danielsen et al., 2009; Kakarougkas et al., 2013). Dr. Kai Ge provided the antibody against PTIP.

Immunofluorescence

U2OS cells grown on glass coverslips were fixed with 3.7 % formaldehyde/PBS for 15 mins at room temperature. Cells were then permeabilized with 0.2 % Triton X-100 in PBS for 5 min at room temperature, blocked with 5 % BSA for 30 min at 37°C and incubated with primary antibodies for 1 h at room temperature. This was followed by three washes with PBS and secondary antibody incubation (Alexa Fluor 568 donkey anti-mouse or Alexa Fluor 647 donkey anti-goat). Next, cells were washed with PBS three times and mounted using vectashield antifade mounting medium with DAPI (H1200; Vector Laboratories).

Microscopy analysis

Images were acquired using a CSU-X spinning disc confocal microscope (Yokogawa, Intelligent Imaging Innovations) on an inverted microscope (DMI600B; Leica), with 63×, 1.4 NA objective lens (mammalian cells), 100×, 1.46 NA objective lens (yeast and mammalian cells) and a charge-coupled device camera (cool-SNAP HQ2, Photometrics) for mammalian cells or electron-multiplying charge-coupled device camera (QuantEM; Photometrics) for yeast cells. SlideBook software (Intelligent Imaging Innovations) was used to obtain Z-stack images. Maximum intensity projections were created in the Slidebook software and exported for analysis in ImageJ software. For the analysis of foci formation of mammalian RIF1 or of FLAG-tagged 53BP1 or CTR-53BP1, more than 150

transfected cells for each condition were imaged and analyzed per replicate. Cells with more than 10 distinct RIF1 or FLAG foci were scored as foci-positive cells. The percentage of RIF1 or FLAG foci-positive cells was calculated based on the arithmetic mean and standard error of the mean (SEM) derived from 3 biological replicates. A two-tailed Student's t-test with 95% confidence interval was used to determine if the difference between the means of two sets of values was significant. For yeast Rfa1 and Rad52 foci analysis, cells were grown in SC-TRP media until log phase (OD = 0.3) and MMS (0.033 %) was added to the cells for 2 h at 30°C. Next, cells were washed in sterile water and resuspended in fresh SC media. Live yeast cultures were mounted on an agarose slide pad (1.2 % agarose in SC–TRP media) and more than 150 cells were scored for each replicate. The percentage of cells with multiple Rad52-mRuby2 foci, or containing a single Rfa1-mRuby2 focus or multiple Rfa1-mRuby2 foci, was calculated based on the arithmetic mean and standard error of the mean (SEM) derived from 3 independent replicates. A two-tailed Student's t-test with 95% confidence interval was used to determine if the difference between the means of two sets of values was significant.

Metaphase spread preparation

HEK293T cells were co-transfected with plasmids for expression of 53BP1 or CTR-53BP1, together with a plasmid for expression of H2B-GFP (Addgene plasmid #11680) used as a marker for transfection. In Flp-In T-REx 293 cells with CTR-53BP1 stably integrated, protein expression was induced using 2 μg/ml doxycycline for 48 h followed by the indicated genotoxin treatment. Cells were then treated with colcemid (150ng/ml) for 1 h and collected by trypsinization followed by centrifugation. Cell pellets were resuspended in hypotonic buffer (0.034 M KCl) for 6 min at 37°C and then fixed in fixation buffer (3:1 of methanol and acetic acid) overnight. Fixed cells were then washed

with fixation buffer three times, spotted onto microscope slide, and mounted using vectashield antifade mounting medium with DAPI. Metaphase spreads were imaged using the CSU-X spinning disc confocal microscope with 100×, 1.46 NA objective. Chromosomal aberrations were then scored. Each condition was repeated at least two times independently and 30-50 metaphases were analyzed per replicate. The two-tailed Student's t-test was used for statistical analysis.

Cell survival assay

HEK293 Flp-In T-REx cells with stably integrated CTR-53BP1 and the control cell line were seeded in doxycycline-containing media for 48 h to induce CTR-53BP1 expression. Cells were then subjected to genotoxin treatment in the continuous presence of doxycycline for 72 h before cells were counted. The percentage of survival was calculated and the graph was plotted based on at least 3 independent experiments showing the mean ± SEM. The two-tailed Student's t-test was used for statistical analysis.

Measurement of resection at HO-induced DSB in yeast

HO-induced DSB resection was measured in JKM139 background by quantitative PCR analysis as described previously (Ferrari et al., 2015). Cells were arrested in G2/M by nocodazole treatment before HO induction. Genomic DNA was extracted and digested or mock-treated with RsaI restriction enzyme (NEB), which cuts inside the amplicons at 0.15 kb, 1.4 kb and 4.8 kb from the HO-cut site, but not in the *PRE1* control region on chromosome V. PCR values are then normalized by the cut efficiency calculated by Southern blot analysis, with a probe around the HO cut site.

SSA repair analysis in yeast

SSA repair efficiency of an HO endonuclease-induced DSB in YMV80 background was analyzed using Southern blotting procedures (Ferrari et al., 2015; Vaze et al., 2002). Briefly, cells grown in YP medium containing 3 % lactate at 28°C reaching a density of 5 × 10^6 cells/ml were arrested with 20 µg/ml nocodazole followed by the addition of 2 % galactose to trigger a single DSB by inducing HO endonuclease expression. Cells remained arrested after DSB induction as confirmed by FACS and monitoring nuclear division (data not shown). At indicated time points, cells were collected to isolate genomic DNA, which was then subjected to Southern blotting analysis to determine the loss of 5' ends at the HO cut *MAT* locus (Clerici et al., 2005; Lee et al., 1998; Vaze et al., 2002). Each experiment was repeated at least three times independently and one representative result is shown.

DR-GFP assay

HEK293 Flp-In T-REx cells with CTR-53BP1 or empty vector stably integrated were cultured in DMEM media containing 2 µg/ml doxycycline and transfected with pDR-GFP (a gift from Maria Jasin, Addgene plasmid #26475) and pCBASceI (a gift from Maria Jasin, Addgene plasmid #26477) (Pierce et al., 1999). In the case of BRCA1 knock-down, cells were transfected with BRCA1 siRNA (BRCA1 HSS101089, Thermo Fisher Scientific) and 48 h post-siRNA transfections cells were transfected with the plasmids pDR-GFP and pCBASceI. The GFP-positive cell population was analyzed 48 h post-transfection. The percentage of GFP-positive cells was quantified in each condition by flow cytometry analysis using FACSAria™ Fusion (BD) and normalized by the control cell line where empty vector was integrated. The data are presented as the mean ± SEM (n>3).

SSA repair assay in mammalian cells

U2OS-SA-GFP cells (kind gift from Jeremy Stark; see (Gunn and Stark, 2012)) were co-transfected with 0.5 µg of I-SceI plasmid and 0.5 µg of plasmid expressing CTR-53BP1 or empty vector using Amaxa Nucleofector II in a 60 mm plate. Cells were grown for 3 days, harvested and subjected to flow cytometry analysis using FACSAria (BD Biosciences) and FACSDiva software to determine the percentage of GFP+ cells.

Measurement of resection at one *Asi*SI-induced DSB in human cells

Resection assay was carried out as described in (Zhou et al., 2014) with some modifications. Briefly, HEK293 cells stably expressing CTR-53BP1 or control cells (stably transfected with an empty vector) were transfected with the pBabe-*Asi*SI–ER plasmid (Iacovoni et al., 2010) using Lipofectamine 3000 (Thermo Fisher Scientific), and selection was performed using 1 µg/ml puromycin. Cells were seeded on a well of a 6 well plate. After 24 h, 2 µg/ml doxycycline was added to induce expression of the CTR-53BP1 protein. Forty-eight h after induction, 300 nM of 4-hydroxy-tomoxifen (4OHT) (Sigma) was added for 6 h to create *Asi*SI-induced DSBs. For experiment with transient expression of CTR-53BP1, U2OS-*Asi*SI-ER cells were transfected with empty vector or the plasmid expressing CTR-53BP1 using Amaxa Nucleofector II. 4OHT was added for 6 h to induce DSBs 48 h post-transfection. To knockdown BRCA1, U2OS-*Asi*SI-ER cells were transfected using Lipofectamine RNAiMax (Thermo Fisher Scientific) and siRNA against BRCA1 (CAGCUACCCUUCCAUCAUAdTdT). After 72 h, cells were treated with 4OHT as described above. After 4OHT treatment, cells were collected and, genomic DNA was extracted and eluted in a final volume of 100 µl using NucleoSpin Tissue kit (Macherey-Nagel). Then, 15 µl of genomic DNA was digested or mock digested with 20 units of BsrGI enzyme (New England Biolabs) in a final volume of 90 µl at 37°C overnight. The mix was incubated at 80°C for 20 min to inactivate the *Bsr*GI enzyme,

and diluted two fold. Five µl of diluted mix from either digested or mock digested sample (about 40 ng) were used as a template in a 25 µl qPCR reaction containing 12.5 µl of 2X master mix containing Syber Green (Genespin) and 0.2 µM of each primer using CFX connect Real Time System (BioRad). Primers listed in Table S7 were used to analyze resection at 335bp and 1618bp from the *Asi*SI cut site on Chromosome 1. The percentage of resection at selected DSB site was determined from qPCR reaction using the formula: *% DSB resected=[100/[(1+2$^{\Delta Ct}$)/2]/f]* (Zierhut and Diffley, 2008) where *ΔCt* is obtained by subtracting *Ct* values of mock digested sample from *Ct* value of digested samples, and *f* is the cut efficiency calculated from qPCR reaction with the primers "Across DSB" using the formula *f*=1-2$^{-\Delta Ct}$ where *ΔCt* is obtained by subtracting *Ct* value of untreated sample from Ct value of 4OHT treated sample.

Figure legends

Figure 1. A competition-based mechanism for the modulation of Rad9 recruitment and DNA end resection via Dpb11 BRCT domains

(A) Working model for the role of Dpb11 in the recruitment of Rad9 to the 5' recessed end of a DNA lesion.

(B) Schematic illustration of the B3/4-Rad9 ($Dpb11^{BRCT3/4}$-Rad9) chimera.

(C) ChIP-qPCR analysis showing the recruitment of B3/4-Rad9 to an HO-induced DSB site. JKM139 derivative strains expressing the indicated chimera proteins, or an untagged Rad9 control, were arrested with nocodazole and HO endonuclease expression was then induced for the indicated time to trigger an irreparable DSB on chromosome III.

(D) HO-induced DSB resection analysis by qPCR in nocodazole-arrested JKM139 derivative strains expressing indicated Rad9 constructs. For (C) and (D) the graph is plotted using mean ± SEM from at least three independent experiments. P value was determined based on single-tailed Student's t test (*for $P<0.05$, ** for $P<0.01$ and *** for $P<0.001$).

(E) Schematic illustration for the SSA (single strand annealing) repair assay measurement. The graph shows the YMV80 Chromosome III region containing HO-cut site. "K" represents *Kpn*I cut sites. The DNA probe hybridizes to sequences within the indicated black boxes. Successful SSA requires 25 kb resection and can be monitored by the appearance of a 3.5 kb SSA product using Southern blot analysis (F) and by cell viability (G).

(H) Working model for the role of the Dpb11-Slx4-Rtt107 complex in antagonizing Rad9 recruitment at lesion sites.

(I) Schematic illustration of the MBD (Minimal multi-BRCT-domain module) chimera.

(J) ChIP-qPCR analysis of B3/4-Rad9 or B3/4(K544A)-Rad9 recruitment to one irreparable HO cut in nocodazole-arrested JKM139 derivative strains expressing the indicated chimeric proteins. The graph is plotted using mean ± SEM from at least two independent experiments.

(K) DSB resection analysis by qPCR to determine the effect of MBD expression on resection efficiency in nocodazole-arrested JKM139 derivative strains expressing Rad9, B3/4-Rad9 or B3/4(K544A)-Rad9. The graph is plotted using mean ± SEM from at least two independent experiments.

(L) Working model for the role of the Slx4-Rtt107 complex in counteracting Dpb11-mediated recruitment of Rad9 to promote DNA-end resection.

For the experiments in Fig. 1, *B3/4-RAD9* and *MBD* chimeras were integrated into the *RAD9* and *SLX4* loci, respectively.

Figure 2. Dpb11-mediated hyper-stabilization of Rad9 impairs proper HR repair of replication-induced lesions.

(A-B) Rfa1-mRuby2 foci were quantified in MMS-treated cells expressing either B3/4-Rad9 chimera or the mutated chimera B3/4(K544A)-Rad9 (fusions were integrated in the *RAD9* locus) or co-overexpressing the MBD and B3/4-Rad9 chimeras. Representative images are shown in (A). Percentage of cells with one Rfa1 focus or multiple Rfa1 foci was quantified and plotted in (B). More than 300 cells were scored per replicate.

(C-D) Rad52-mRuby2 foci were quantified in cells expressing either B3/4-Rad9 or the mutated chimera B3/4(K544A)-Rad9 or co-overexpressing the MBD and B3/4-Rad9 chimeras. Cells were analyzed after treatment with 0.033 % MMS for 2 h or following recovery of cells for 2 h in fresh media after MMS treatment. Cells were evaluated based on the presence or the absence of Rad52-mRuby2 foci. More than 300 cells were

scored per replicate. Representative images were shown in (C). The percentage of cells with Rad52 foci were quantified and plotted in (D)

(E) MMS sensitivity of wild-type cells expressing MBD and/or B3/4-Rad9 from plasmids. Four-fold serial dilutions were spotted on SC-URA-TRP plates and grown for 2–3 days at 30°C.

(F) MMS sensitivity of wild-type cells expressing either B3/4-Rad9 or B3/4 (K544A)-Rad9. Four-fold serial dilutions were spotted on SC-URA-TRP plates and grown for 2–3 days at 30°C.

(G) Immunoblots showing the phosphorylation status of Rad53 and B3/4-Rad9 in cells expressing Rad9 or B3/4-Rad9 or co-expressing B3/4-Rad9 with MBD. The Rad9 fusions were integrated at the *RAD9* locus and MBD was expressed from a plasmid (pMBS910).

For (A), (B) and (F), B3/4-Rad9 chimera was integrated into the *RAD9* locus. Graph is plotted using mean ± SEM from at least three independent experiments. *P* value is determined based on two-tailed Student's t test (*for $P<0.05$, ** for $P<0.01$ and *** for $P<0.001$).

Figure 3. Phosphorylation of Slx4 by Mec1 promotes DNA end resection.

(A) Co-IP of Dpb11 with Slx4 or Rad9 in wild-type or *mec1Δ* cells treated with 0.01% MMS for 3 h.

(B) Co-IP of Dpb11 with Slx4 or Rad9 in wild-type or *mec1Δ* cells arrested with 7 μg/ml nocodazole for 3 h followed by phleomycin treatment (40 μg/ml) for 15 min in the continuous presence of nocodazole.

(C) DSB resection analysis by qPCR of indicated nocodazole-arrested JKM139 derivative strains. The graph is plotted using mean ± SEM from at least two independent

experiments.

(D) A model for the role of Dpb11 in resection control via coordination of Slx4 and Rad9.

Figure 4. Proteomic analysis of TOPBP1 interactions modulated by replication stress.

(A) Quantitative mass spectrometry analysis of TOPBP1 interactions in cells arrested with HU or nocodazole. HEK293T cells were grown in “light” and “heavy” SILAC media and treated with 1 mM hydroxyurea (HU) for 24 h to identify proteins that interact with TOPBP1 in response to replication stress. Two independent experiments were performed, one pulling down endogenous TOPBP1 with an anti-TOPBP1 antibody another pulling down over-expressed HA-TOPBP1 with anti-HA resin. Proteins with a TOPBP1-IP / mock-IP ratio above 4 in both experiments were considered specific TOPBP1 interactors. Each dot in dark color represents an identified TOPBP1 interaction. Similar procedures were performed in cells treated with 100 ng/ml nocodazole for 14 h to define TOPBP1 interactions in G2/M.

(B) Quantitative mass spectrometry analysis of changes in TOPBP1 interactions in HEK293T cells treated with HU (grown in “light” SILAC media) or treated with nocodazole (grown in “heavy” SILAC media).

(C) Co-IP of TOPBP1 with BRCA1 or 53BP1 in HEK293T cells treated with HU (1mM) or nocodazole (100 ng/ml) as described in Fig. 3A.

(D) Co-IP experiment determining the contribution of each pair of BRCT domains in TOPBP1 for stabilizing interactions with BRCA1 and 53BP1. HEK293T cells were transfected with plasmids containing TOPBP1 (wild-type and the following mutants: BRCT-1: K154A and K155A; BRCT-5: K704A and W711R; BRCT-7: R1314Q) or empty vector (see plasmid list) and treated with 1 mM HU for 24 h.

(E) Co-IP of TOPBP1 with BRCA1 or 53BP1 in the presence of ATR, ATM or DNA-PK

inhibitors. HEK293T cells transfected with HA-TOPBP1 were pre-treated with ATR, ATM or DNA-PK inhibitors as indicated for 45 min followed by 30 min HU treatment in the presence of inhibitors.

(F) Depiction of an analogous mode of TOPBP1^{Dpb11} interactions with pro-HR (BRCA1 in humans and Slx4 in yeast) and anti-resection (53BP1^{Rad9}) factors.

Figure 5. Hyper-stabilization of the TOPBP1-53BP1 interaction promotes 53BP1 recruitment and impairs HR-mediated repair.

(A) Schematic illustration of the CTR-53BP1 chimera in which a 120 amino acid fragment in the N-terminal domain of RFC1 was fused to full-length 53BP1.

(B) Co-IP experiment pulling-down CTR-53BP1 and probing for TOPBP1 and PTIP in HEK293T cells treated with 1 mM HU for 24 h. Ectopic 53BP1 and CTR-53BP1 containing an N-terminal FLAG-tag were transiently over-expressed.

(C) Immunofluorescence of U2OS cells transfected with FLAG-53BP1 or FLAG-CTR-53BP1 and treated with 1 mM HU for 24 h followed by a 3 h release in fresh media. We note that in our experience, this short release period enhances the visualization of replication stress-induced nuclear foci for the indicated proteins. White dotted lines indicate nuclear boundaries. Displayed images were extracted from the panels in Fig. S2A showing scale bars and DAPI staining.

(D) Quantitation of results from the experiment shown in (Fig. 5C) scoring FLAG and RIF1 foci in transfection-positive cells. Graphs represent results from at least 3 independent experiments and more than 150 transfected cells were scored per replicate.

(E) Analysis of chromosomal abnormalities in metaphases of HEK293T cells treated with 1 μM ATR inhibitor and/or 3 μM PARP inhibitor AZD2461. Metaphase spreads were prepared as described in Material and Methods section. n>45 metaphases were analyzed in each replicate.

(F) Immunoblot showing the doxycycline-induced expression of CTR-53BP1. CTR-53BP1 is stably integrated in HEK293 cells using Flp-In T-REx system where CTR-53BP1 can be inducibly expressed upon treatment of doxycycline.

(G-H) Analysis of metaphase chromosomal abnormalities in HEK293 cells expressing CTR-53BP1 in response to PARP inhibitor. Cells were treated with doxycycline for 48 h and 3 μM AZD2461 was added for another 24 h. Cells were then analyzed for chromosomal aberrations. (G) Total chromosomal aberrations (breaks, fusions, acentrics, radials) and (H) subset of radial chromosomes per metaphase. n>30 metaphases were analyzed in each replicate and each condition was repeated at least 3 times.

(I) HR efficiency was measured in CTR-53BP1-expressing cells using the DR-GFP reporter system. HEK293 cells with CTR-53BP1 stably integrated were treated with doxycycline and transfected with both the pDR-GFP and pCBASceI plasmids. GFP+ cell population was analyzed by flow cytometry 48 h post-transfection and the percentage of GFP+ cells were calculated in each condition. The data are normalized to the control cell line stably integrated with an empty vector and are presented as the mean ± SEM (n > 3).

(J) Efficiency of SSA-mediated repair was measured in cells transiently expressing CTR-53BP1 or empty vector. U2OS SA-GFP cells were co-transfected with plasmids expressing CTR-53BP1 and I-SceI. GFP+ cells were then analyzed 72 h post-transfection as described in (I).

(K) Measurement of DSB resection in cells expressing CTR-53BP1 by qPCR. HEK293 cells with both CTR-53BP1 and *Asi*SI-ER stably integrated were treated with doxycycline for 48 h followed by 4OHT treatment for another 6h to induce DSB.

(L-M) Analysis of metaphase chromosomal abnormalities in HEK293 cells with DOX-inducible CTR-53BP1 upon depletion of BRCA1. HEK293 cells with CTR-53BP1 stably integrated were transfected with BRCA1 siRNA or control siRNA. At 48 h post-transfection, cells were treated with 3 μM AZD2461 for 24 h and then harvested. Total

number of chromosomal aberrations (M) and radial chromosomes (N) were scored. BRCA1 knock-down efficiency is shown in Fig. S5B.

(N) Model for the role of TOPBP1 in mediating a phosphorylation-regulated circuitry for the control of recombinational DNA repair. See text for details.

All graphs displayed in Fig. 5 were plotted using mean ± SEM from at least three independent experiments. *P* value is determined based on two-tailed Student's t test (*for $P<0.05$, ** for $P<0.01$ and *** for $P<0.001$).

REFERENCES

Abreu, C.M., R. Kumar, D. Hamilton, A.W. Dawdy, K. Creavin, S. Eivers, K. Finn, J.L. Balsbaugh, R. O'Connor, P.A. Kiely, J. Shabanowitz, D.F. Hunt, M. Grenon, and N.F. Lowndes. 2013. Site-specific phosphorylation of the DNA damage response mediator rad9 by cyclin-dependent kinases regulates activation of checkpoint kinase 1. *PLoS genetics*. 9:e1003310.

Bastos de Oliveira, F.M., D. Kim, J.R. Cussiol, J. Das, M.C. Jeong, L. Doerfler, K.H. Schmidt, H. Yu, and M.B. Smolka. 2015. Phosphoproteomics reveals distinct modes of Mec1/ATR signaling during DNA replication. *Mol Cell*. 57:1124-1132.

Boos, D., L. Sanchez-Pulido, M. Rappas, L.H. Pearl, A.W. Oliver, C.P. Ponting, and J.F. Diffley. 2011. Regulation of DNA replication through Sld3-Dpb11 interaction is conserved from yeast to humans. *Curr Biol*. 21:1152-1157.

Bothmer, A., D.F. Robbiani, N. Feldhahn, A. Gazumyan, A. Nussenzweig, and M.C. Nussenzweig. 2010. 53BP1 regulates DNA resection and the choice between classical and alternative end joining during class switch recombination. *J Exp Med*. 207:855-865.

Bouwman, P., A. Aly, J.M. Escandell, M. Pieterse, J. Bartkova, H. van der Gulden, S. Hiddingh, M. Thanasoula, A. Kulkarni, Q. Yang, B.G. Haffty, J. Tommiska, C. Blomqvist, R. Drapkin, D.J. Adams, H. Nevanlinna, J. Bartek, M. Tarsounas, S. Ganesan, and J. Jonkers. 2010. 53BP1 loss rescues BRCA1 deficiency and is associated with triple-negative and BRCA-mutated breast cancers. *Nat Struct Mol Biol*. 17:688-695.

Bunting, S.F., E. Callen, N. Wong, H.T. Chen, F. Polato, A. Gunn, A. Bothmer, N. Feldhahn, O. Fernandez-Capetillo, L. Cao, X. Xu, C.X. Deng, T. Finkel, M. Nussenzweig, J.M. Stark, and A. Nussenzweig. 2010. 53BP1 inhibits homologous recombination in Brca1-deficient cells by blocking resection of DNA breaks. *Cell*. 141:243-254.

Callen, E., M. Di Virgilio, M.J. Kruhlak, M. Nieto-Soler, N. Wong, H.T. Chen, R.B. Faryabi, F. Polato, M. Santos, L.M. Starnes, D.R. Wesemann, J.E. Lee, A. Tubbs, B.P. Sleckman, J.A. Daniel, K. Ge, F.W. Alt, O. Fernandez-Capetillo, M.C. Nussenzweig, and A. Nussenzweig. 2013. 53BP1 mediates productive and mutagenic DNA repair through distinct phosphoprotein interactions. *Cell*. 153:1266-1280.

Cao, L., X. Xu, S.F. Bunting, J. Liu, R.H. Wang, L.L. Cao, J.J. Wu, T.N. Peng, J. Chen, A. Nussenzweig, C.X. Deng, and T. Finkel. 2009. A selective requirement for 53BP1 in the biological response to genomic instability induced by Brca1 deficiency. *Mol Cell*. 35:534-541.

Carr, A.M., and S. Lambert. 2013. Replication stress-induced genome instability: the dark side of replication maintenance by homologous recombination. *J Mol Biol*. 425:4733-4744.

Cescutti, R., S. Negrini, M. Kohzaki, and T.D. Halazonetis. 2010. TopBP1 functions with 53BP1 in the G1 DNA damage checkpoint. *EMBO J*. 29:3723-3732.

Chapman, J.R., P. Barral, J.B. Vannier, V. Borel, M. Steger, A. Tomas-Loba, A.A. Sartori, I.R. Adams, F.D. Batista, and S.J. Boulton. 2013. RIF1 is essential for 53BP1-dependent nonhomologous end joining and suppression of DNA double-strand break resection. *Mol Cell*. 49:858-871.

Chapman, J.R., A.J. Sossick, S.J. Boulton, and S.P. Jackson. 2012a. BRCA1-

associated exclusion of 53BP1 from DNA damage sites underlies temporal control of DNA repair. *J Cell Sci*. 125:3529-3534.
Chapman, J.R., M.R. Taylor, and S.J. Boulton. 2012b. Playing the end game: DNA double-strand break repair pathway choice. *Molecular cell*. 47:497-510.
Chen, X., D. Cui, A. Papusha, X. Zhang, C.D. Chu, J. Tang, K. Chen, X. Pan, and G. Ira. 2012. The Fun30 nucleosome remodeller promotes resection of DNA double-strand break ends. *Nature*. 489:576-580.
Chin, J.K., V.I. Bashkirov, W.D. Heyer, and F.E. Romesberg. 2006. Esc4/Rtt107 and the control of recombination during replication. *DNA Repair (Amst)*. 5:618-628.
Clerici, M., D. Mantiero, G. Lucchini, and M.P. Longhese. 2005. The Saccharomyces cerevisiae Sae2 protein promotes resection and bridging of double strand break ends. *J Biol Chem*. 280:38631-38638.
Clerici, M., C. Trovesi, A. Galbiati, G. Lucchini, and M.P. Longhese. 2014. Mec1/ATR regulates the generation of single-stranded DNA that attenuates Tel1/ATM signaling at DNA ends. *EMBO J*. 33:198-216.
Cussiol, J.R., C.M. Jablonowski, A. Yimit, G.W. Brown, and M.B. Smolka. 2015. Dampening DNA damage checkpoint signalling via coordinated BRCT domain interactions. *EMBO J*. 34:1704-1717.
Danielsen, J.M., D.H. Larsen, K.B. Schou, R. Freire, J. Falck, J. Bartek, and J. Lukas. 2009. HCLK2 is required for activity of the DNA damage response kinase ATR. *J Biol Chem*. 284:4140-4147.
Deng, C.X., and R.H. Wang. 2003. Roles of BRCA1 in DNA damage repair: a link between development and cancer. *Hum Mol Genet*. 12 Spec No 1:R113-123.
Di Virgilio, M., E. Callen, A. Yamane, W. Zhang, M. Jankovic, A.D. Gitlin, N. Feldhahn, W. Resch, T.Y. Oliveira, B.T. Chait, A. Nussenzweig, R. Casellas, D.F. Robbiani, and M.C. Nussenzweig. 2013. Rif1 prevents resection of DNA breaks and promotes immunoglobulin class switching. *Science*. 339:711-715.
Dibitetto, D., M. Ferrari, C.C. Rawal, A. Balint, T. Kim, Z. Zhang, M.B. Smolka, G.W. Brown, F. Marini, and A. Pellicioli. 2016. Slx4 and Rtt107 control checkpoint signalling and DNA resection at double-strand breaks. *Nucleic Acids Res*.
Escribano-Diaz, C., A. Orthwein, A. Fradet-Turcotte, M. Xing, J.T. Young, J. Tkac, M.A. Cook, A.P. Rosebrock, M. Munro, M.D. Canny, D. Xu, and D. Durocher. 2013. A cell cycle-dependent regulatory circuit composed of 53BP1-RIF1 and BRCA1-CtIP controls DNA repair pathway choice. *Mol Cell*. 49:872-883.
Feng, L., K.W. Fong, J. Wang, W. Wang, and J. Chen. 2013. RIF1 counteracts BRCA1-mediated end resection during DNA repair. *J Biol Chem*. 288:11135-11143.
Ferrari, M., D. Dibitetto, G. De Gregorio, V.V. Eapen, C.C. Rawal, F. Lazzaro, M. Tsabar, F. Marini, J.E. Haber, and A. Pellicioli. 2015. Functional interplay between the 53BP1-ortholog Rad9 and the Mre11 complex regulates resection, end-tethering and repair of a double-strand break. *PLoS Genet*. 11:e1004928.
Fricke, W.M., and S.J. Brill. 2003. Slx1-Slx4 is a second structure-specific endonuclease functionally redundant with Sgs1-Top3. *Genes Dev*. 17:1768-1778.
Gaillard, H., T. Garcia-Muse, and A. Aguilera. 2015. Replication stress and cancer. *Nat Rev Cancer*. 15:276-289.
Gelot, C., I. Magdalou, and B.S. Lopez. 2015. Replication stress in Mammalian cells and its consequences for mitosis. *Genes*. 6:267-298.
Germann, S.M., V.H. Oestergaard, C. Haas, P. Salis, A. Motegi, and M. Lisby. 2011. Dpb11/TopBP1 plays distinct roles in DNA replication, checkpoint response and homologous recombination. *DNA Repair (Amst)*. 10:210-224.
Granata, M., F. Lazzaro, D. Novarina, D. Panigada, F. Puddu, C.M. Abreu, R. Kumar, M. Grenon, N.F. Lowndes, P. Plevani, and M. Muzi-Falconi. 2010. Dynamics of

Rad9 chromatin binding and checkpoint function are mediated by its dimerization and are cell cycle-regulated by CDK1 activity. *PLoS Genet*. 6.
Greenberg, R.A., B. Sobhian, S. Pathania, S.B. Cantor, Y. Nakatani, and D.M. Livingston. 2006. Multifactorial contributions to an acute DNA damage response by BRCA1/BARD1-containing complexes. *Genes Dev*. 20:34-46.
Gritenaite, D., L.N. Princz, B. Szakal, S.C. Bantele, L. Wendeler, S. Schilbach, B.H. Habermann, J. Matos, M. Lisby, D. Branzei, and B. Pfander. 2014. A cell cycle-regulated Slx4-Dpb11 complex promotes the resolution of DNA repair intermediates linked to stalled replication. *Genes Dev*. 28:1604-1619.
Gunn, A., and J.M. Stark. 2012. I-SceI-based assays to examine distinct repair outcomes of mammalian chromosomal double strand breaks. *Methods Mol Biol*. 920:379-391.
Heyer, W.D. 2015. Regulation of recombination and genomic maintenance. *Cold Spring Harb Perspect Biol*. 7:a016501.
Iacovoni, J.S., P. Caron, I. Lassadi, E. Nicolas, L. Massip, D. Trouche, and G. Legube. 2010. High-resolution profiling of gammaH2AX around DNA double strand breaks in the mammalian genome. *EMBO J*. 29:1446-1457.
Kakarougkas, A., A. Ismail, Y. Katsuki, R. Freire, A. Shibata, and P.A. Jeggo. 2013. Co-operation of BRCA1 and POH1 relieves the barriers posed by 53BP1 and RAP80 to resection. *Nucleic Acids Res*. 41:10298-10311.
Kolodner, R.D., C.D. Putnam, and K. Myung. 2002. Maintenance of genome stability in Saccharomyces cerevisiae. *Science*. 297:552-557.
Kumar, R., and C.F. Cheok. 2014. RIF1: a novel regulatory factor for DNA replication and DNA damage response signaling. *DNA Repair (Amst)*. 15:54-59.
Lazzaro, F., V. Sapountzi, M. Granata, A. Pellicioli, M. Vaze, J.E. Haber, P. Plevani, D. Lydall, and M. Muzi-Falconi. 2008. Histone methyltransferase Dot1 and Rad9 inhibit single-stranded DNA accumulation at DSBs and uncapped telomeres. *EMBO J*. 27:1502-1512.
Lee, S.E., J.K. Moore, A. Holmes, K. Umezu, R.D. Kolodner, and J.E. Haber. 1998. Saccharomyces Ku70, mre11/rad50 and RPA proteins regulate adaptation to G2/M arrest after DNA damage. *Cell*. 94:399-409.
Liu, Y., and M.B. Smolka. 2016. TOPBP1 takes RADical command in recombinational DNA repair. *J Cell Biol*. 212:263-266.
Manke, I.A., D.M. Lowery, A. Nguyen, and M.B. Yaffe. 2003. BRCT repeats as phosphopeptide-binding modules involved in protein targeting. *Science*. 302:636-639.
Morin, I., H.P. Ngo, A. Greenall, M.K. Zubko, N. Morrice, and D. Lydall. 2008. Checkpoint-dependent phosphorylation of Exo1 modulates the DNA damage response. *EMBO J*. 27:2400-2410.
Morishima, K., S. Sakamoto, J. Kobayashi, H. Izumi, T. Suda, Y. Matsumoto, H. Tauchi, H. Ide, K. Komatsu, and S. Matsuura. 2007. TopBP1 associates with NBS1 and is involved in homologous recombination repair. *Biochem Biophys Res Commun*. 362:872-879.
Moudry, P., K. Watanabe, K.M. Wolanin, J. Bartkova, I.E. Wassing, S. Watanabe, R. Strauss, R. Troelsgaard Pedersen, V.H. Oestergaard, M. Lisby, M. Andujar-Sanchez, A. Maya-Mendoza, F. Esashi, J. Lukas, and J. Bartek. 2016. TOPBP1 regulates RAD51 phosphorylation and chromatin loading and determines PARP inhibitor sensitivity. *J Cell Biol*. 212:281-288.
Munoz, I.M., P.A. Jowsey, R. Toth, and J. Rouse. 2007. Phospho-epitope binding by the BRCT domains of hPTIP controls multiple aspects of the cellular response to DNA damage. *Nucleic acids research*. 35:5312-5322.

Navadgi-Patil, V.M., and P.M. Burgers. 2008. Yeast DNA replication protein Dpb11 activates the Mec1/ATR checkpoint kinase. *J Biol Chem*.

Ohouo, P.Y., F.M. Bastos de Oliveira, B.S. Almeida, and M.B. Smolka. 2010. DNA damage signaling recruits the Rtt107-Slx4 scaffolds via Dpb11 to mediate replication stress response. *Mol Cell*. 39:300-306.

Ohouo, P.Y., F.M. Bastos de Oliveira, Y. Liu, C.J. Ma, and M.B. Smolka. 2013. DNA-repair scaffolds dampen checkpoint signalling by counteracting the adaptor Rad9. *Nature*. 493:120-124.

Orthwein, A., S.M. Noordermeer, M.D. Wilson, S. Landry, R.I. Enchev, A. Sherker, M. Munro, J. Pinder, J. Salsman, G. Dellaire, B. Xia, M. Peter, and D. Durocher. 2015. A mechanism for the suppression of homologous recombination in G1 cells. *Nature*. 528:422-426.

Pfander, B., and J.F. Diffley. 2011. Dpb11 coordinates Mec1 kinase activation with cell cycle-regulated Rad9 recruitment. *EMBO J*. 30:4897-4907.

Pierce, A.J., R.D. Johnson, L.H. Thompson, and M. Jasin. 1999. XRCC3 promotes homology-directed repair of DNA damage in mammalian cells. *Genes Dev*. 13:2633-2638.

Prakash, R., Y. Zhang, W. Feng, and M. Jasin. 2015. Homologous recombination and human health: the roles of BRCA1, BRCA2, and associated proteins. *Cold Spring Harb Perspect Biol*. 7:a016600.

Puddu, F., M. Granata, L. Di Nola, A. Balestrini, G. Piergiovanni, F. Lazzaro, M. Giannattasio, P. Plevani, and M. Muzi-Falconi. 2008. Phosphorylation of the budding yeast 9-1-1 complex is required for Dpb11 function in the full activation of the UV-induced DNA damage checkpoint. *Mol Cell Biol*. 28:4782-4793.

Roberts, T.M., M.S. Kobor, S.A. Bastin-Shanower, M. Ii, S.A. Horte, J.W. Gin, A. Emili, J. Rine, S.J. Brill, and G.W. Brown. 2006. Slx4 regulates DNA damage checkpoint-dependent phosphorylation of the BRCT domain protein Rtt107/Esc4. *Mol Biol Cell*. 17:539-548.

Rodriguez, M., X. Yu, J. Chen, and Z. Songyang. 2003. Phosphopeptide binding specificities of BRCA1 COOH-terminal (BRCT) domains. *J Biol Chem*. 278:52914-52918.

Schwartz, E.K., and W.D. Heyer. 2011. Processing of joint molecule intermediates by structure-selective endonucleases during homologous recombination in eukaryotes. *Chromosoma*. 120:109-127.

Segurado, M., and J.F. Diffley. 2008. Separate roles for the DNA damage checkpoint protein kinases in stabilizing DNA replication forks. *Genes Dev*. 22:1816-1827.

Tak, Y.S., Y. Tanaka, S. Endo, Y. Kamimura, and H. Araki. 2006. A CDK-catalysed regulatory phosphorylation for formation of the DNA replication complex Sld2-Dpb11. *EMBO J*. 25:1987-1996.

Tanaka, S., T. Umemori, K. Hirai, S. Muramatsu, Y. Kamimura, and H. Araki. 2007. CDK-dependent phosphorylation of Sld2 and Sld3 initiates DNA replication in budding yeast. *Nature*. 445:328-332.

Tang, J., N.W. Cho, G. Cui, E.M. Manion, N.M. Shanbhag, M.V. Botuyan, G. Mer, and R.A. Greenberg. 2013. Acetylation limits 53BP1 association with damaged chromatin to promote homologous recombination. *Nat Struct Mol Biol*. 20:317-325.

Vaze, M.B., A. Pellicioli, S.E. Lee, G. Ira, G. Liberi, A. Arbel-Eden, M. Foiani, and J.E. Haber. 2002. Recovery from checkpoint-mediated arrest after repair of a double-strand break requires Srs2 helicase. *Mol Cell*. 10:373-385.

Wang, G., X. Tong, S. Weng, and H. Zhou. 2012. Multiple phosphorylation of Rad9 by CDK is required for DNA damage checkpoint activation. *Cell Cycle*. 11:3792-

3800.
White, C.I., and J.E. Haber. 1990. Intermediates of recombination during mating type switching in Saccharomyces cerevisiae. *EMBO J*. 9:663-673.
Yamane, K., X. Wu, and J. Chen. 2002. A DNA damage-regulated BRCT-containing protein, TopBP1, is required for cell survival. *Mol Cell Biol*. 22:555-566.
Yoo, H.Y., A. Kumagai, A. Shevchenko, A. Shevchenko, and W.G. Dunphy. 2009. The Mre11-Rad50-Nbs1 complex mediates activation of TopBP1 by ATM. *Molecular biology of the cell*. 20:2351-2360.
Yu, X., C.C. Chini, M. He, G. Mer, and J. Chen. 2003. The BRCT domain is a phospho-protein binding domain. *Science*. 302:639-642.
Zegerman, P., and J.F. Diffley. 2007. Phosphorylation of Sld2 and Sld3 by cyclin-dependent kinases promotes DNA replication in budding yeast. *Nature*. 445:281-285.
Zhang, H., H. Liu, Y. Chen, X. Yang, P. Wang, T. Liu, M. Deng, B. Qin, C. Correia, S. Lee, J. Kim, M. Sparks, A.A. Nair, D.L. Evans, K.R. Kalari, P. Zhang, L. Wang, Z. You, S.H. Kaufmann, Z. Lou, and H. Pei. 2016. A cell cycle-dependent BRCA1-UHRF1 cascade regulates DNA double-strand break repair pathway choice. *Nature communications*. 7:10201.
Zhou, Y., P. Caron, G. Legube, and T.T. Paull. 2014. Quantitation of DNA double-strand break resection intermediates in human cells. *Nucleic Acids Res*. 42:e19.
Zierhut, C., and J.F. Diffley. 2008. Break dosage, cell cycle stage and DNA replication influence DNA double strand break response. *EMBO J*. 27:1875-1885.
Zimmermann, M., F. Lottersberger, S.B. Buonomo, A. Sfeir, and T. de Lange. 2013. 53BP1 regulates DSB repair using Rif1 to control 5' end resection. *Science*. 339:700-704.

Figure 1

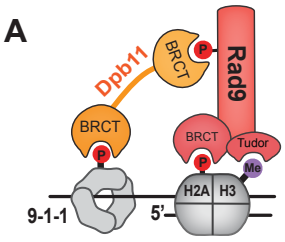
A
Dpb11
BRCT
Rad9
BRCT
BRCT
Tudor
P
Me
H2A
H3
9-1-1
5'

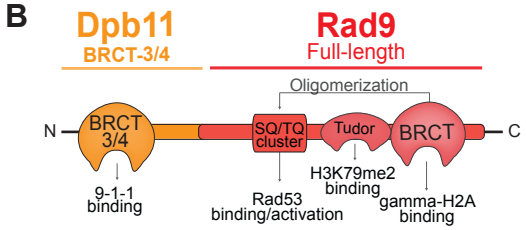
B
Dpb11
BRCT-3/4
Rad9
Full-length
Oligomerization
N
BRCT 3/4
SQ/TQ cluster
Tudor
BRCT
C
9-1-1 binding
Rad53 binding/activation
H3K79me2 binding
gamma-H2A binding

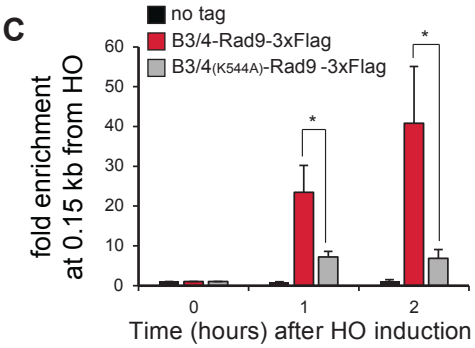
C
no tag
B3/4-Rad9-3xFlag
B3/4(K544A)-Rad9 -3xFlag
fold enrichment at 0.15 kb from HO
Time (hours) after HO induction

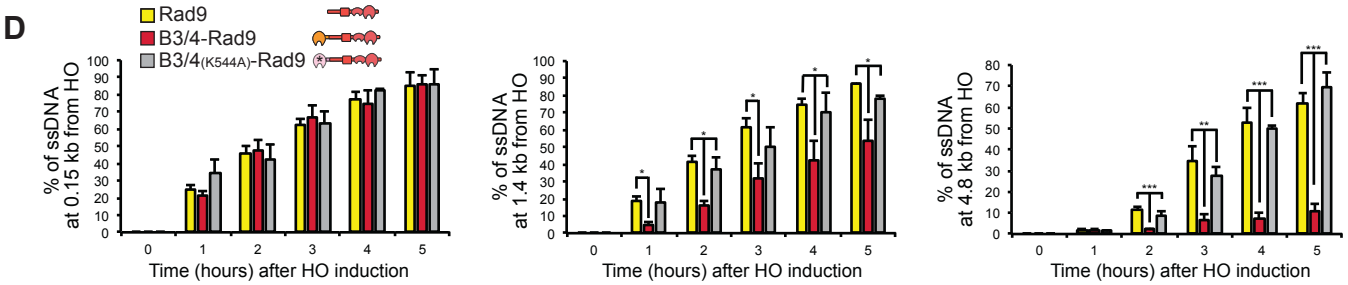
D
Rad9
B3/4-Rad9
B3/4(K544A)-Rad9
% of ssDNA at 0.15 kb from HO
% of ssDNA at 1.4 kb from HO
% of ssDNA at 4.8 kb from HO
Time (hours) after HO induction

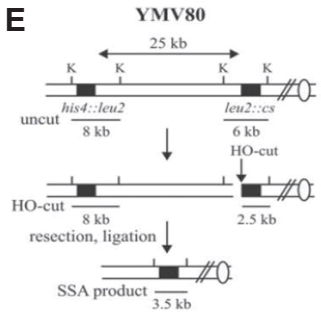
E
YMV80
25 kb
K
his4::leu2
leu2::cs
uncut
8 kb
6 kb
HO-cut
2.5 kb
resection, ligation
SSA product
3.5 kb

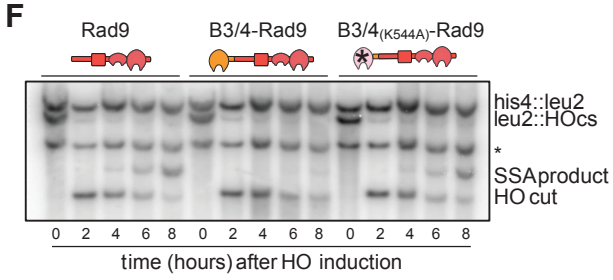
F
Rad9
B3/4-Rad9
B3/4(K544A)-Rad9
his4::leu2
leu2::HOcs
*
SSAproduct
HO cut
time (hours) after HO induction

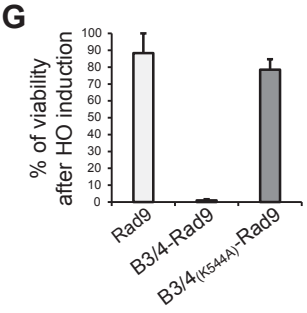
G
% of viability after HO induction
Rad9
B3/4-Rad9
B3/4(K544A)-Rad9

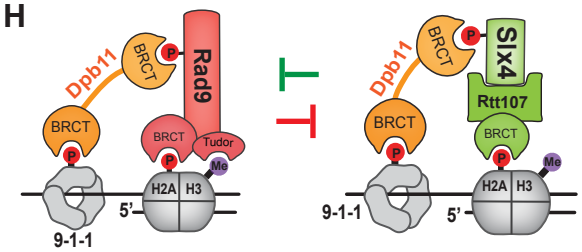
H
Dpb11
BRCT
Rad9
BRCT
BRCT
Tudor
P
Me
H2A
H3
9-1-1
5'
Six4
Rtt107

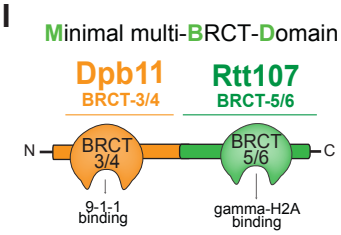
I
Minimal multi-BRCT-Domain
Dpb11
BRCT-3/4
Rtt107
BRCT-5/6
N
BRCT 3/4
BRCT 5/6
C
9-1-1 binding
gamma-H2A binding

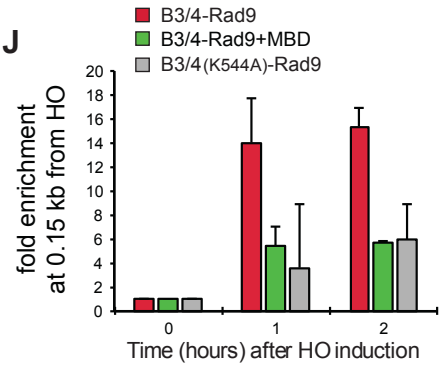
J
B3/4-Rad9
B3/4-Rad9+MBD
B3/4(K544A)-Rad9
fold enrichment at 0.15 kb from HO
Time (hours) after HO induction

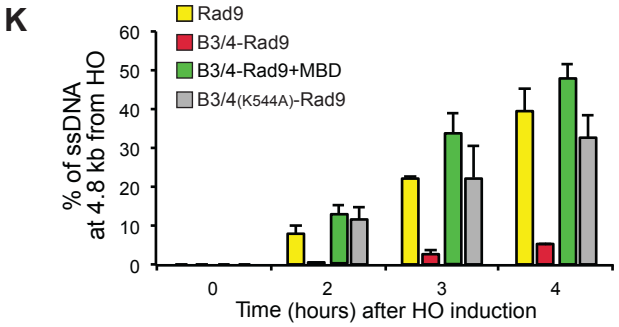
K
Rad9
B3/4-Rad9
B3/4-Rad9+MBD
B3/4(K544A)-Rad9
% of ssDNA at 4.8 kb from HO
Time (hours) after HO induction

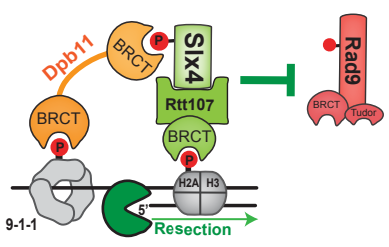
L
Dpb11
BRCT
Six4
Rtt107
Rad9
BRCT
Tudor
P
H2A
H3
9-1-1
5'
Resection

Figure 2

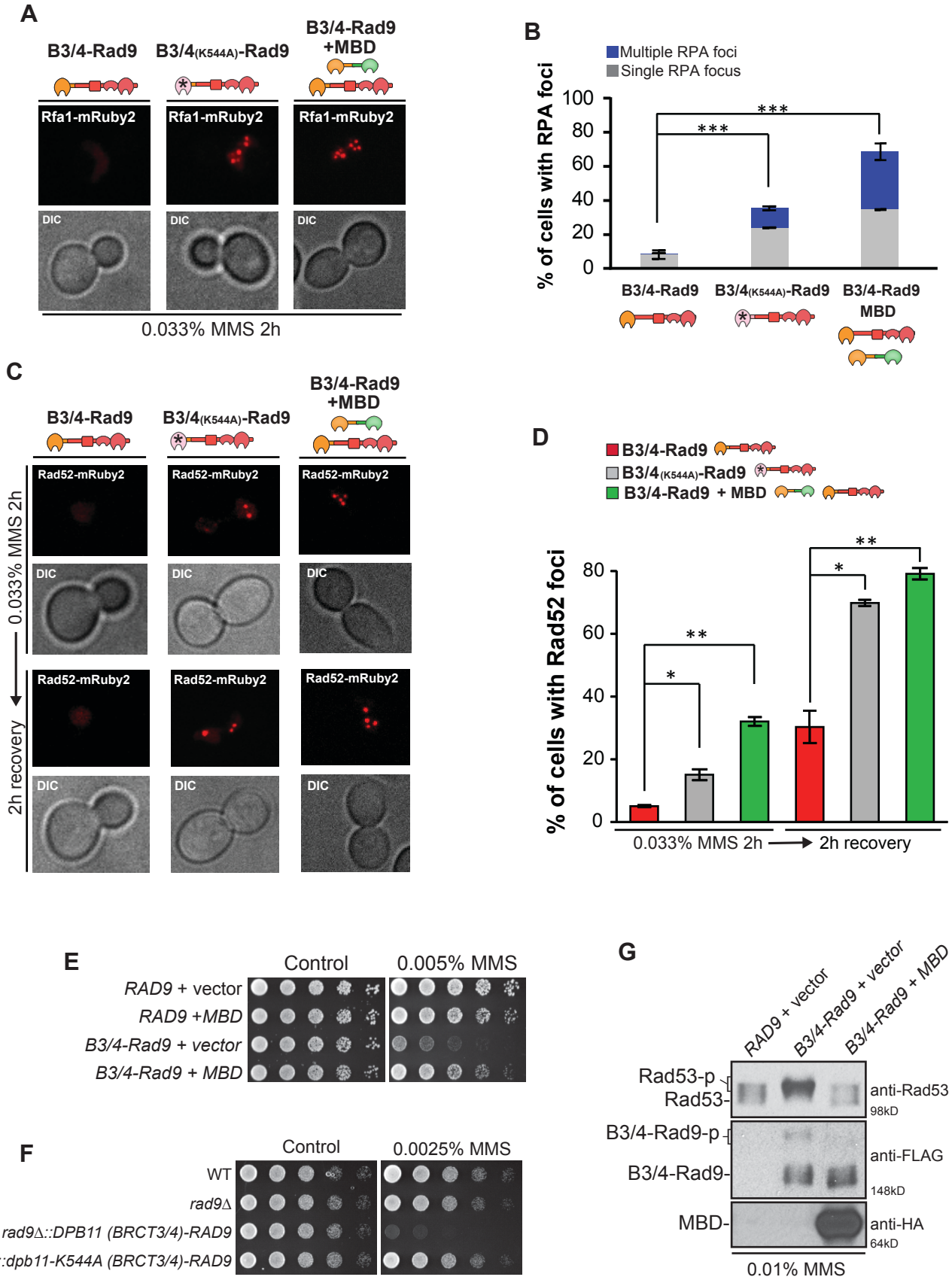
A
B3/4-Rad9
B3/4(K544A)-Rad9
B3/4-Rad9 +MBD
Rfa1-mRuby2
DIC
0.033% MMS 2h
B
Multiple RPA foci
Single RPA focus
% of cells with RPA foci
100
80
60
40
20
0
***
***
B3/4-Rad9
B3/4(K544A)-Rad9
B3/4-Rad9 MBD
C
B3/4-Rad9
B3/4(K544A)-Rad9
B3/4-Rad9 +MBD
Rad52-mRuby2
DIC
0.033% MMS 2h
2h recovery
D
B3/4-Rad9
B3/4(K544A)-Rad9
B3/4-Rad9 + MBD
% of cells with Rad52 foci
80
60
40
20
0
**
*
**
*
0.033% MMS 2h
2h recovery
E
Control
0.005% MMS
RAD9 + vector
RAD9 +MBD
B3/4-Rad9 + vector
B3/4-Rad9 + MBD
F
Control
0.0025% MMS
WT
rad9Δ
rad9Δ::DPB11 (BRCT3/4)-RAD9
rad9Δ::dpb11-K544A (BRCT3/4)-RAD9
G
RAD9 + vector
B3/4-Rad9 + vector
B3/4-Rad9 + MBD
Rad53-p
Rad53-
anti-Rad53
98kD
B3/4-Rad9-p
B3/4-Rad9-
anti-FLAG
148kD
MBD-
anti-HA
64kD
0.01% MMS

Figure 3

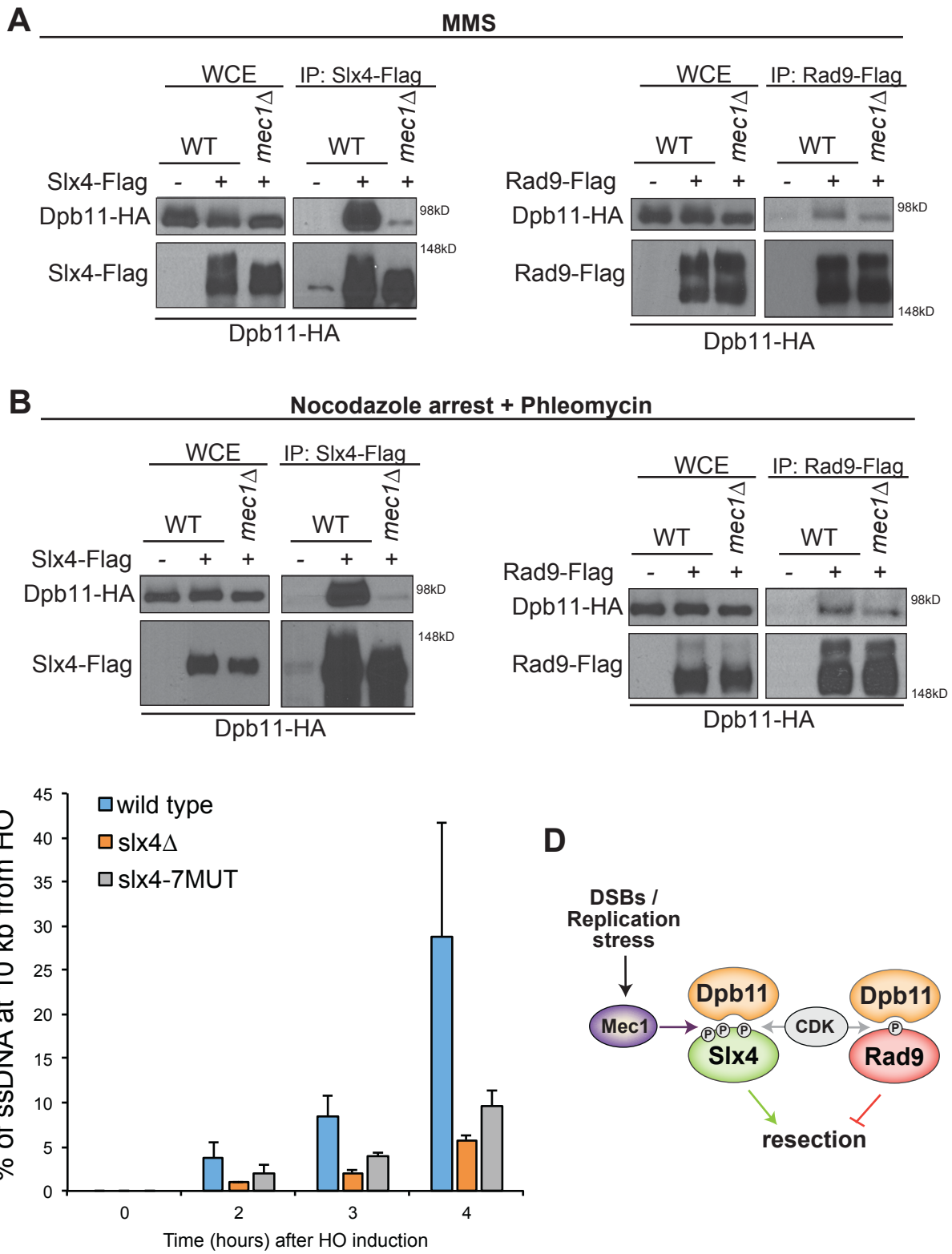
A
MMS
WCE
IP: Slx4-Flag
WT
mec1Δ
Slx4-Flag
Dpb11-HA
98kD
148kD
IP: Rad9-Flag
Rad9-Flag
B
Nocodazole arrest + Phleomycin
C
% of ssDNA at 10 kb from HO
wild type
slx4Δ
slx4-7MUT
Time (hours) after HO induction
D
DSBs / Replication stress
Mec1
Dpb11
Slx4
CDK
Rad9
resection

Figure 4

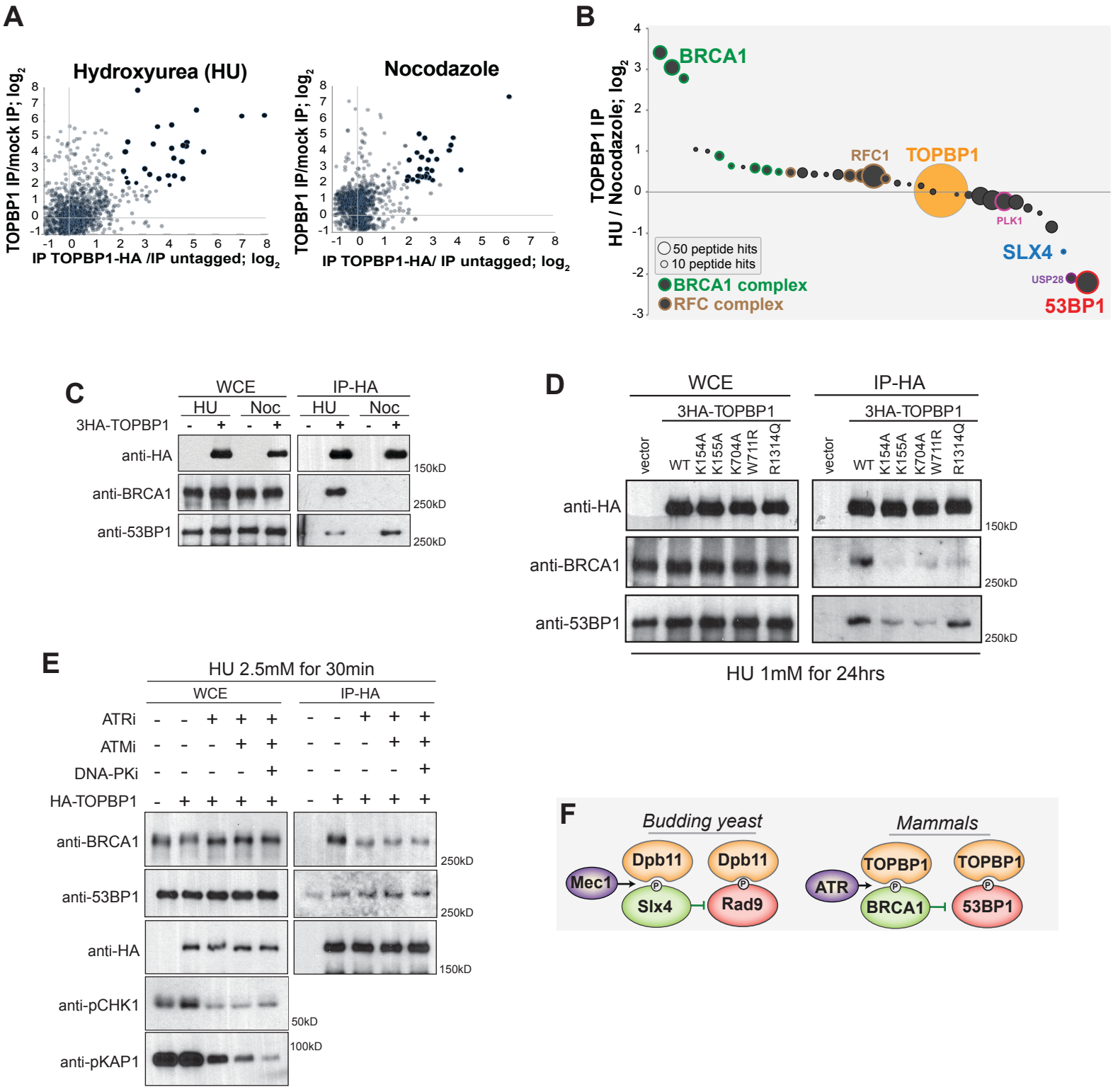
A
Hydroxyurea (HU)
Nocodazole
TOPBP1 IP/mock IP; log2
IP TOPBP1-HA /IP untagged; log2
IP TOPBP1-HA/ IP untagged; log2
B
TOPBP1 IP
HU / Nocodazole; log2
BRCA1
RFC1
TOPBP1
PLK1
SLX4
USP28
53BP1
50 peptide hits
10 peptide hits
BRCA1 complex
RFC complex
C
WCE
IP-HA
HU
Noc
3HA-TOPBP1
anti-HA
anti-BRCA1
anti-53BP1
150kD
250kD
D
WCE
IP-HA
3HA-TOPBP1
vector
WT
K154A
K155A
K704A
W711R
R1314Q
anti-HA
anti-BRCA1
anti-53BP1
150kD
250kD
HU 1mM for 24hrs
E
HU 2.5mM for 30min
WCE
IP-HA
ATRi
ATMi
DNA-PKi
HA-TOPBP1
anti-BRCA1
anti-53BP1
anti-HA
anti-pCHK1
anti-pKAP1
250kD
150kD
50kD
100kD
F
Budding yeast
Mammals
Mec1
Dpb11
Slx4
Rad9
ATR
TOPBP1
BRCA1
53BP1

Figure 5

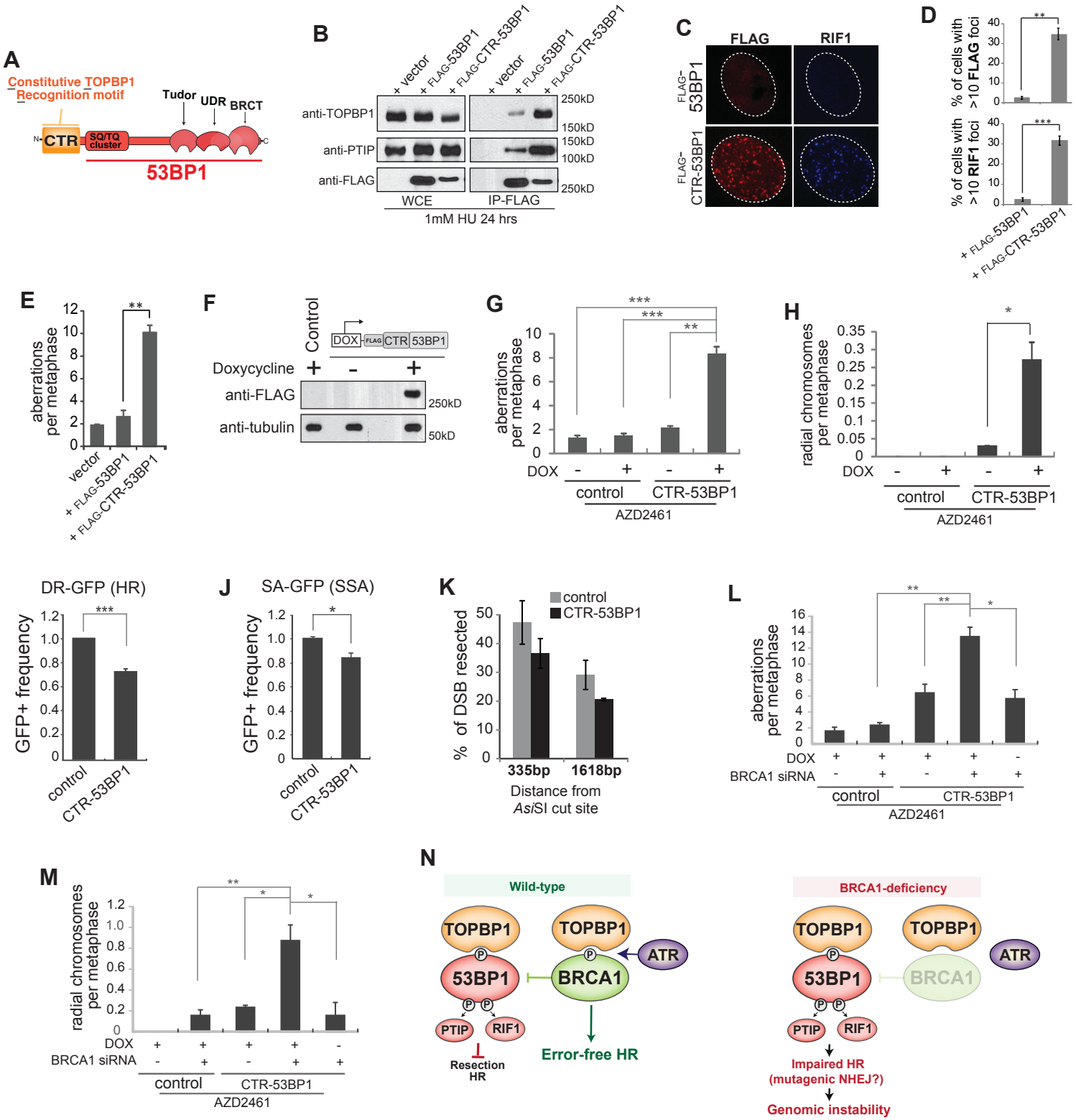
A
Constitutive TOPBP1 Recognition motif
Tudor
UDR
BRCT
N-CTR
SQ/TQ cluster
C
53BP1
B
+ vector
+ FLAG-53BP1
+ FLAG-CTR-53BP1
anti-TOPBP1
anti-PTIP
anti-FLAG
250kD
150kD
100kD
WCE
IP-FLAG
1mM HU 24 hrs
C
FLAG
RIF1
FLAG-53BP1
FLAG-CTR-53BP1
D
% of cells with >10 FLAG foci
% of cells with >10 RIF1 foci
E
aberrations per metaphase
vector
+ FLAG-53BP1
+ FLAG-CTR-53BP1
F
Control
DOX
FLAG
CTR
53BP1
Doxycycline
anti-FLAG
anti-tubulin
250kD
50kD
G
aberrations per metaphase
DOX
control
CTR-53BP1
AZD2461
H
radial chromosomes per metaphase
DOX
control
CTR-53BP1
AZD2461
I
DR-GFP (HR)
GFP+ frequency
control
CTR-53BP1
J
SA-GFP (SSA)
GFP+ frequency
control
CTR-53BP1
K
control
CTR-53BP1
% of DSB resected
335bp
1618bp
Distance from AsiSI cut site
L
aberrations per metaphase
DOX
BRCA1 siRNA
control
CTR-53BP1
AZD2461
M
radial chromosomes per metaphase
DOX
BRCA1 siRNA
control
CTR-53BP1
AZD2461
N
Wild-type
TOPBP1
53BP1
PTIP
RIF1
BRCA1
ATR
Resection
HR
Error-free HR
BRCA1-deficiency
Impaired HR
(mutagenic NHEJ?)
Genomic instability

Supplemental material

Summary:

Fig. S1 shows that BRCA1 and 53BP1 are not detected in pull-downs of 53BP1 and BRCA1, respectively, and that their interaction with TOPBP1 is oppositely regulated by HU. Fig. S2 demonstrates that CTR-53BP1 promotes the recruitment of the NHEJ factor RIF1 to DNA damage foci. Fig. S3 presents the characterization of a HEK293 stable cell line generated for doxycycline-inducible expression of CTR-53BP1. Fig. S4 shows that expression of CTR-53BP1 leads to a stronger impairment in HR compared to overexpression of 53BP1. Fig. S5 shows the data used for determining the effect of CTR-53BP1 expression and BRCA1 depletion on the accumulation of chromosomal aberrations. Tables S1 and S2 describe the yeast strains and plasmids used in this study, respectively. Tables S3 and S4 show the mass spectrometry analysis results of TOPBP1 interactions in cells arrested by HU and nocodazole, respectively. Table S5 shows the mass spectrometry analysis result comparing TOPBP1 interactions in HU versus nocodazole. Table S6 lists the oligonucleotide sequences used for ChIP and DSB resection analysis in yeast. Table S7 lists the oligonucleotide sequences used for the measurement of DSB resection in human cell lines.

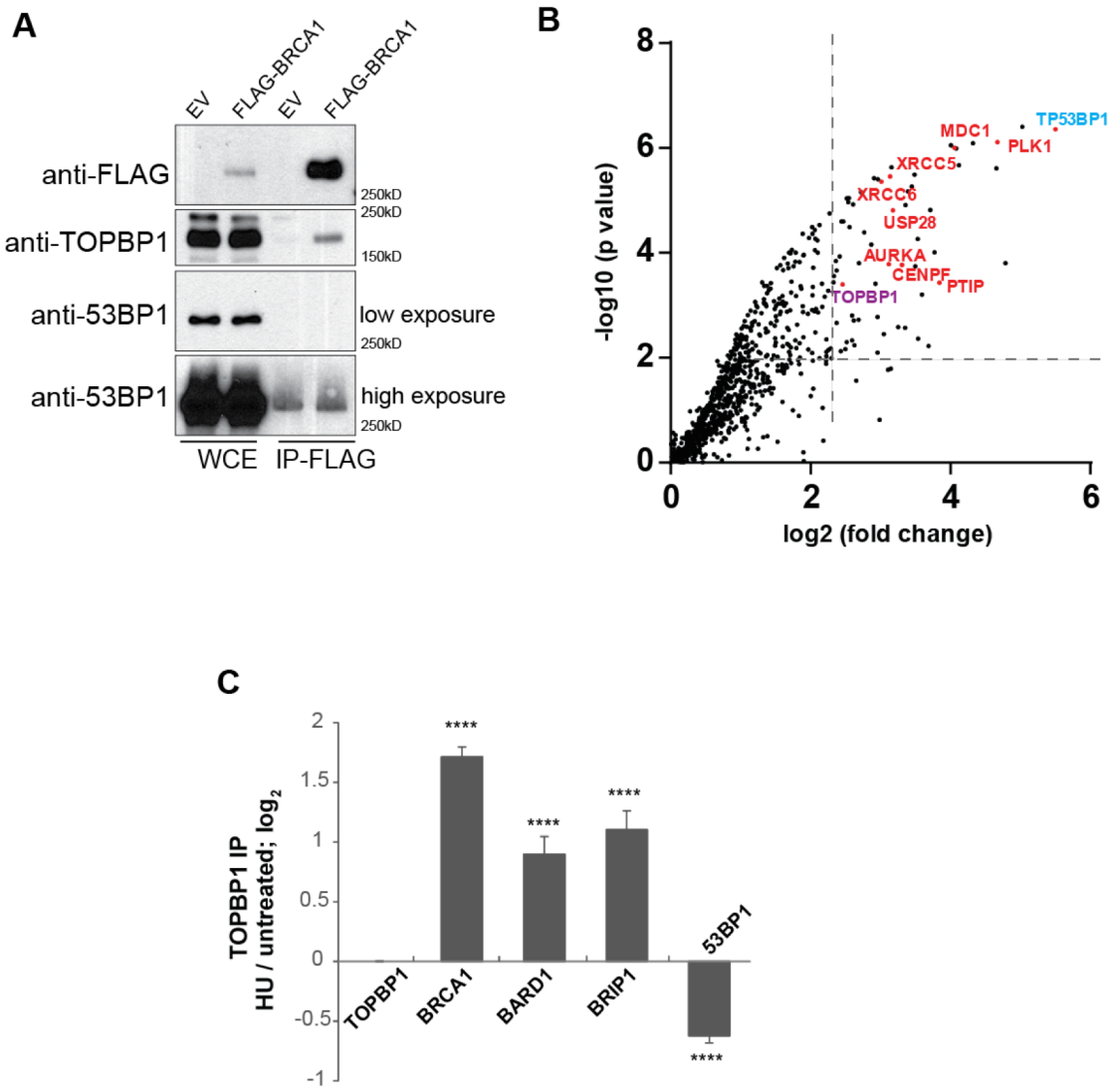

Figure S1 BRCA1 and 53BP1 are not detected in pulldowns of 53BP1 and BRCA1, respectively, and their interaction with TOPBP1 is oppositely regulated by HU.

(A) Co-IP of BRCA1 for monitoring interaction with TOPBP1 or 53BP1. HEK293T cells were transfected with FLAG-BRCA1 and 48 h post-transfection, cells were treated with 1 mM HU for 24 h. BRCA1 was pulled-down using anti-FLAG resin and immunoprecipitates were probed for both TOPBP1 and 53BP1.

(B) Volcano plot for the quantitative mass spectrometry analysis of 53BP1 interactions in cells treated with HU for 24 h (of note, we were unable to perform a similar co-IP experiment shown in (A) for 53BP1 pulldowns due to a cross-reactive band when using the anti-BRCA1 antibody in 53BP1 immunoprecipitates). HEK293T cells were grown in “light” and “heavy” SILAC DMEM media and transfected with empty vector or a plasmid expressing FLAG-53BP1, respectively. Both “heavy” and “light” cells were then treated with HU for 24 h and harvested. Following anti-FLAG pull-down, eluates from 53BP1-IP and mock-IP were combined and subjected to quantitative mass spectrometry analysis. While TOPBP1 was detected, BRCA1 was not detected as a 53BP1-interacting protein in this analysis.

(C) Quantitative mass spectrometry analysis of changes in TOPBP1 interactions in HEK293T cells treated with HU for 24 h (grown in “light” SILAC media) or untreated (asynchronously grown in “heavy” SILAC media). Endogenous TOPBP1 was pulled down using anti-TOPBP1 antibody and the immunoprecipitates were then subjected to mass spectrometry analysis. Error bars represent the variation of the HU/untreated ratios of the multiple peptides detected in the experiment. The significance of the ratio difference between the identified TOPBP1-interacting proteins and TOPBP1 is determined by comparing the HU/untreated ratios of each TOPBP1-interacting protein with that of TOPBP1 using the Mann–Whitney U test (*for P<0.05, ** for P<0.01, *** for P<0.001, **** for P<0.0001).

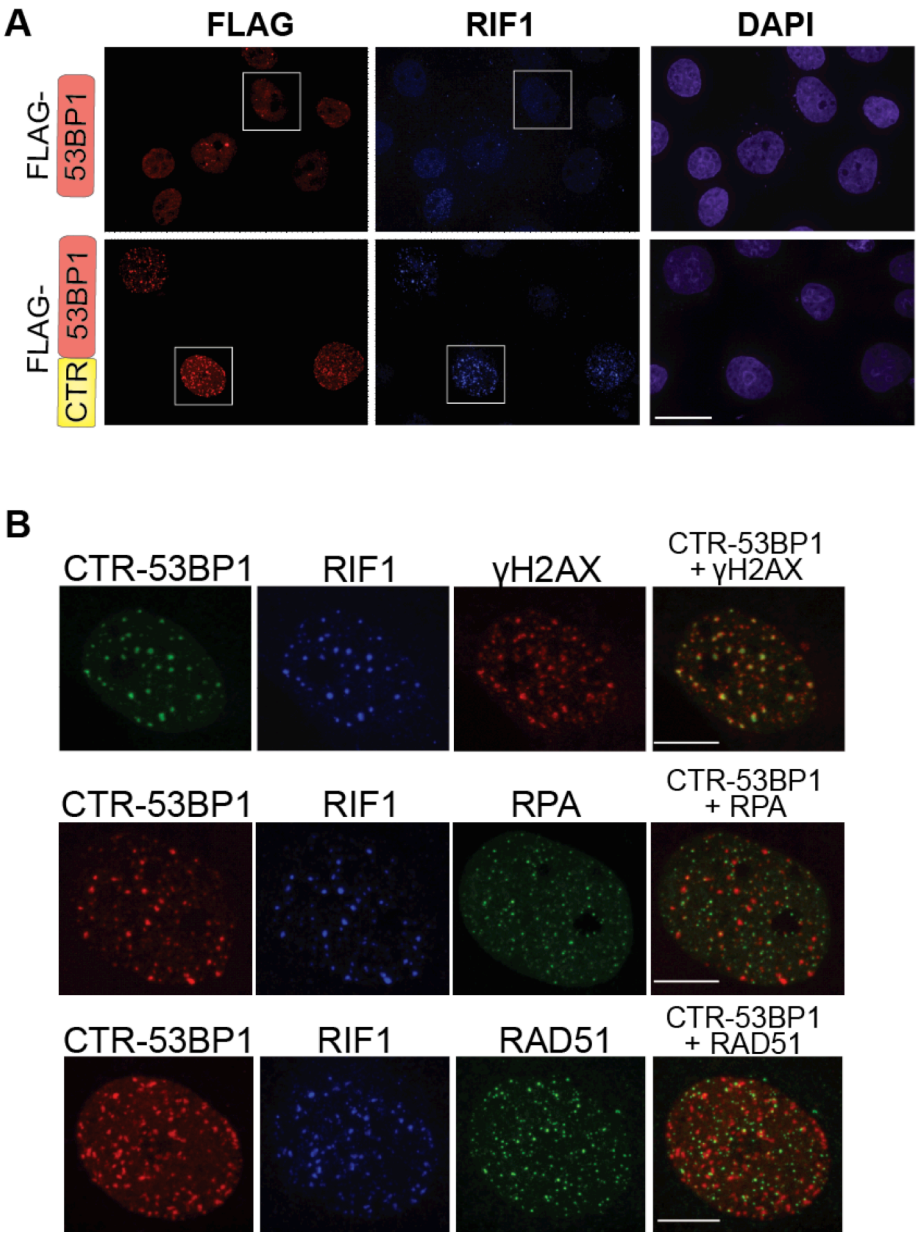

Figure S2 CTR-53BP1 promotes the recruitment of RIF1 to DNA damage foci, and does not co-localize with HR-associated proteins RPA and RAD51.

(A) Immunofluorescence of U2OS cells transfected with FLAG-53BP1 or FLAG-CTR-53BP1 and treated with 1 mM HU for 24 h followed by a 3 h release in fresh media. After genotoxin treatment, cells were fixed and stained using anti-FLAG and anti-RIF1 antibodies. More than 150 transfection positive cells were imaged and scored for CTR-53BP1 or RIF1 foci. White boxes indicate regions that were zoomed in and shown in Fig. 5C. Scale bar, 30μm. The percentage of cells with more than 10 FLAG or RIF1 foci were quantified and shown in Fig. 5D.

(B) Representative confocal images of U2OS cells transiently transfected with FLAG-CTR-53BP1 and co-stained with γ-H2AX, RIF1, RPA and/or RAD51. Scale bar, 10μm. Cells were treated with 1 mM HU for 24 h followed by a 3 h release in fresh media. Cells were then fixed and stained using anti-FLAG and anti-RIF1 together with anti-γ-H2AX or anti-RPA or anti-RAD51. FLAG-CTR-53BP1 co-localizes with γ-H2AX and RIF1, but not with RPA or RAD51.

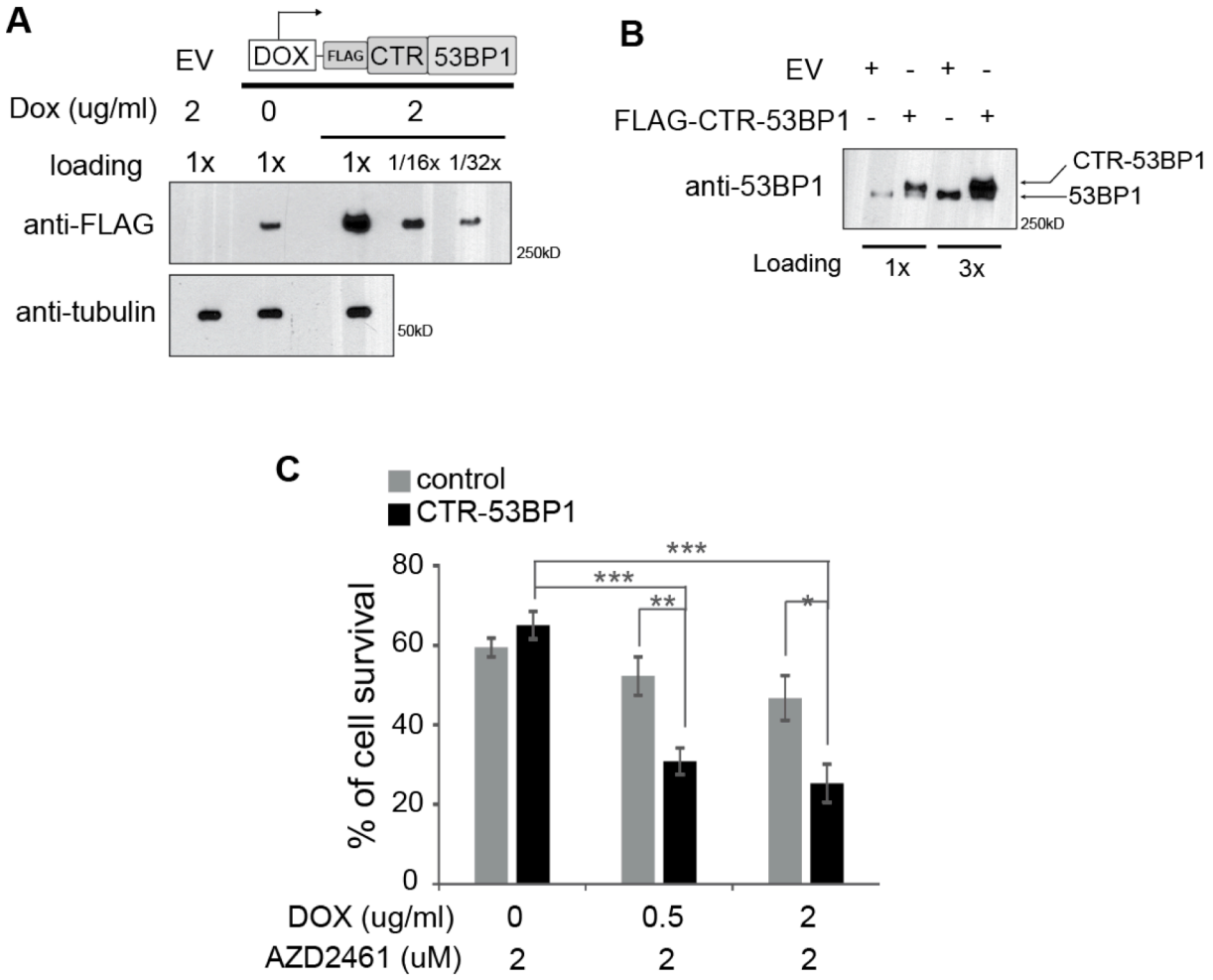

Figure S3 Characterization of a HEK293 stable cell line for doxycycline-inducible expression of CTR-53BP1.

(A) Western blots showing doxycycline (DOX) inducible expression of CTR-53BP1 in HEK293 Flp-In T-REx cells with CTR-53BP1 stably integrated. Cells were treated with 2 μg/ml DOX for 48 h before harvested for protein preparation. Different amounts of the DOX-induced CTR-53BP1 sample were loaded in order to quantify the leakage expression of CTR-53BP1 in cells not subjected to DOX treatment. The indicated blot is a higher exposure of the blot shown in Fig. 5F.

(B) Western blot comparing the level of DOX-induced CTR-53BP1 expression with the level of endogenous 53BP1 expression in control HEK293 Flp-In T-REx cells where an empty vector was used for stable integration. Cells were treated with 2 μg/ml DOX for 48 h and protein extracts we used for western blot analysis using antibodies against 53BP1.

(C) Cellular sensitivity to PARP inhibitor (AZD2461) induced by the expression of CTR-53BP1. Flp-In T-REx HEK293 cells with CTR-53BP1 stably integrated and the control cell line (with empty vector stably integrated) were grown in DOX-containing media for 48 h before treatment with PARP inhibitor for another 72 h in the presence of DOX. Cells were then counted after genotoxin treatment. The data are presented as mean ± SEM based on 3 independent experiments. *P* value is determined based on two-tailed Student's t test (*for $P<0.05$, ** for $P<0.01$ and *** for $P<0.001$).

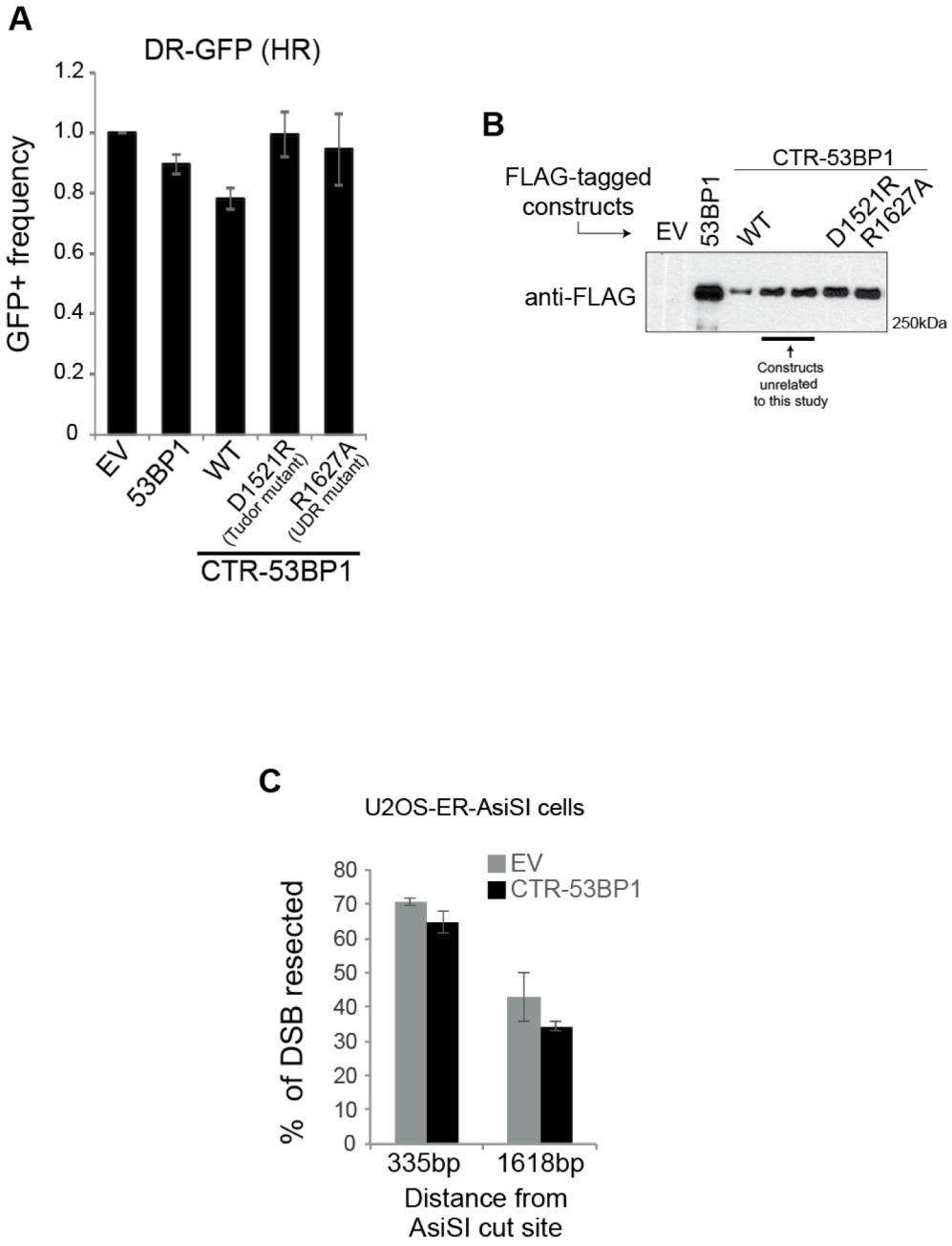

Figure S4 Expression of CTR-53BP1 leads to a stronger impairment in HR compared to overexpression of 53BP1.

(A) Measurement of HR efficiency by the DR-GFP assay in HEK293 cells over-expressing full length 53BP1, CTR-53BP1 or CTR-53BP1 mutants harboring mutations in the UDR or tudor domains. HEK293 Flp-In T-REx cells were transiently co-transfected with pDR-GFP/pCBASce and plasmids for over-expression of wildtype 53BP1, CTR-53BP1, CTR-53BP1 D1521R (tudor mutant) or CTR-53BP1 R1627A (UDR mutant). GFP positive cell population was analyzed by flow cytometry 48 h post-transfection and the percentage of GFP+ cells was calculated in each condition. The data are normalized to control cells transfected with empty vector (EV) and presented as mean ± SEM based on at least 3 independent experiments.

(B) Western blot comparing the expression level of transiently expressed 53BP1, CTR-53BP1, CTR-53BP1 D1521R (tudor mutant) and CTR-53BP1 R1627A (UDR mutant). (C) Measurement of resection at one *Asi*SI-induced DSB in U2OS-ER-*Asi*SI cells transiently over-expressing CTR-53BP1 (see Materials and Methods for details).

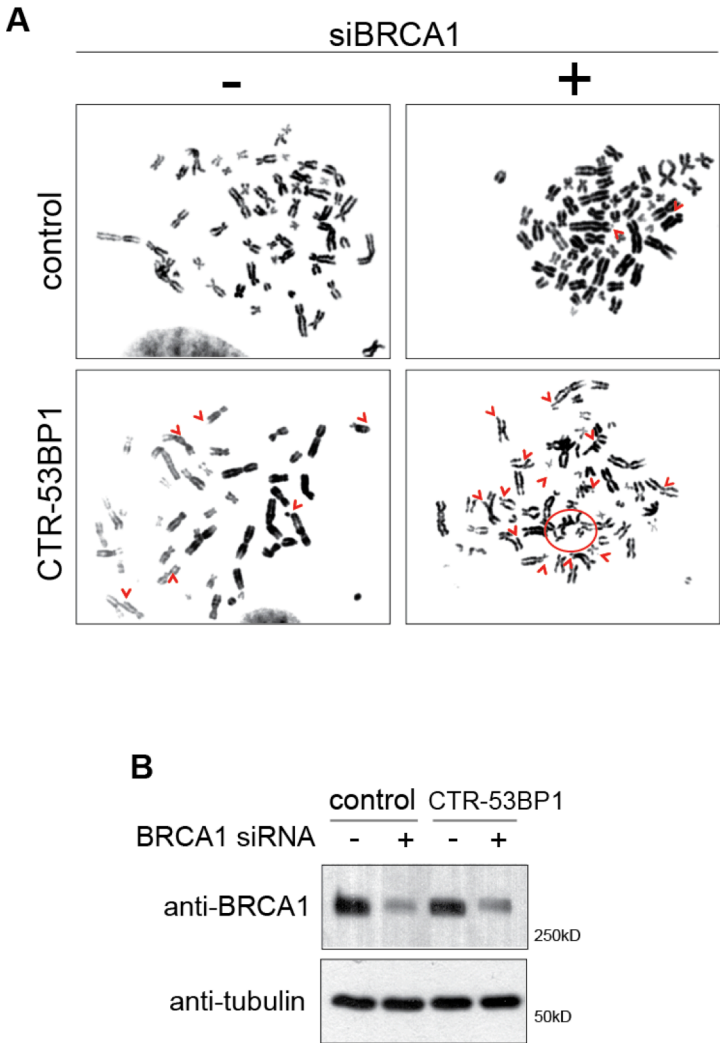

Figure S5 Effect of CTR-53BP1 expression and BRCA1 depletion on the accumulation of chromosomal aberrations.

(A) Representative images of metaphase spreads of HEK293 Flp-In T-REx cells stably expressing CTR-53BP1 with BRCA1 concomitantly depleted. HEK293 Flp-In T-REx cells with DOX-inducible CTR-53BP1 stably integrated, or the control cell line (with empty vector stably integrated), were grown in media containing 2 μg/ml DOX and transfected with control siRNA or siRNA against BRCA1. After 48 h of transfection, cells were treated with 3 μM PARP inhibitor (AZD2461) for 24 h before harvested for metaphase spread preparation. Red "V" marks indicate scored chromosomal aberrations.

(B) Western blot showing the knockdown efficiency of BRCA1 in HEK293 Flp-In T-REx cells with CTR-53BP1 or the empty vector stably integrated.

Table S1. Genotype of yeast strains used in this study.

Strain No.	Relevant Genotype	Reference
MBS164	*MATa, ura3-52, leu2Δ1, trp1Δ63, his3Δ200, lys2ΔBgl, hom3-10, ade2Δ1, ade8, arg4Δ, sml1Δ::TRP1, bar1Δ::HIS3*	(Ohouo et al., 2010)
MBS448	*MATa, ura3-52, leu2Δ1, trp1Δ63, his3Δ200, lys2ΔBgl, hom3-10, ade2Δ1, ade8, arg4Δ, sml1Δ::TRP1, bar1Δ::HIS3, DPB11-6xHIS-3xHA::LEU2*	(Ohouo et al., 2010)
MBS571	*MATa, ura3-52, leu2Δ1, trp1Δ63, his3Δ200, lys2ΔBgl, hom3-10, ade2Δ1, ade8, arg4Δ, sml1Δ::TRP1, bar1Δ::HIS3, DPB11-6xHIS-3xHA-LEU2, SLX4-6xHIS-3xFLAG::kanMX6*	(Ohouo et al., 2010)
MBS1050	*ura3-52 trp1Δ63, his3Δ200*	This study
MBS1053	*ura3-52 trp1Δ63, his3Δ200, rad9Δ::URA3*	This study
MBS1551	*MATa, ura3-52, leu2Δ1, trp1Δ63, his3Δ200, lys2ΔBgl, hom3-10, ade2Δ1, ade8, arg4Δ, sml1Δ::TRP1, bar1Δ::HIS3, DPB11-6xHIS-3xHA::LEU2, RAD9-6xHIS-3xFLAG::kanMX6*	(Ohouo et al., 2013)
MBS2867	*ura3-52, trp1Δ63, his3Δ200, pRAD9-DPB11(292-600aa)-RAD9-6xHIS-3xFLAG::kanMX6*	This study
MBS2869	*ura3-52, trp1Δ63, his3Δ200, pRAD9-dpb11-K544A(292-600aa)-RAD9-6xHIS-3xFLAG::kanMX6*	This study
Y1600 (JKM139)	MATa *ho hml::ADE1 hmr::ADE1 ade1-100 leu2-3, 112 lys5, trp1::hisG, ura3-52, lys5::ade3::GAL10::HO*	Pellicioli's lab
MBS2901 (JKM139)	MATa *ho hml::ADE1 hmr::ADE1 ade1-100 leu2-3, 112 lys5, trp1::hisG, ura3-52, lys5::ade3::GAL10::HO, rad9Δ::HPH*	Pellicioli's lab
MBS2931	*ura3-52, trp1Δ63, his3Δ200, pRAD9-DPB11(292-600aa)-RAD9-GFP::HIS3, RAD52-mRUBY2::kanMX6*	This study
MBS2933	*ura3-52, trp1Δ63, his3Δ200, pRAD9-dpb11-K544A(292-600aa)-RAD9-GFP::HIS3, RAD52-mRUBY2::kanMX6*	This study
MBS2935	*MATa ho hml::ADE1 hmr::ADE1 ade1-100 leu2-3, 112 lys5, trp1::hisG, ura3-52, lys5::ade3::GAL10::HO, pRAD9-DPB11(292-600aa)-RAD9-3xFLAG::kanMX6*	This study
MBS2937	*MATa ho hml::ADE1 hmr::ADE1 ade1-100 leu2-3, 112 lys5, trp1::hisG, ura3-52, lys5::ade3::GAL10::HO, pRAD9-dpb11-K544A(292-600aa)-RAD9-3xFLAG::kanMX6*	This study
MBS2939	*MATa ho hml::ADE1 hmr::ADE1 ade1-100 leu2-3, 112 lys5, trp1::hisG, ura3-52, lys5::ade3::GAL10::HO, pRAD9-DPB11(292-600aa)-RAD9-3xFLAG::natMX*	
MBS2958	*ura3-52, trp1Δ63, his3Δ200, pRAD9-DPB11(292-600aa)-RAD9-GFP::HIS3, RFA1-mRUBY2::kanMX6*	This study
MBS2960	*ura3-52, trp1Δ63, his3Δ200, pRAD9-dpb11-K544A(292-600aa)-RAD9-GFP::HIS3, RFA1-mRUBY2::kanMX6*	This study
MBS2986	MATa, *ura3-52, leu2Δ1, trp1Δ63, his3Δ200, lys2ΔBgl, hom3-10, ade2Δ1, ade8, arg4Δ, sml1Δ::TRP1, bar1Δ::HIS3, DPB11-6HIS3HA::LEU2, SLX4-6xHis-3xFLAG::kanMX6, mec1Δ::natMX*	This study
MBS2988	MATa, *ura3-52, leu2Δ1, trp1Δ63, his3Δ200, lys2ΔBgl, hom3-10, ade2Δ1, ade8, arg4Δ, sml1Δ::TRP1, bar1Δ::HIS3, DPB11-6HIS3HA::LEU2, RAD9-6xHis-3xFLAG::kanMX6, mec1Δ::natMX*	This study
MBS2941	*MATa ho hml::ADE1 hmr::ADE1 ade1-100 leu2-3, 112 lys5, trp1::hisG, ura3-52, lys5::ade3::GAL10::HO, pRAD9-dpb11-K544A(292-600aa)-RAD9-3xFLAG::natMX*	This study
MBS2998	*MATa ho hml::ADE1 hmr::ADE1 ade1-100 leu2-3, 112 lys5, trp1::hisG, ura3-52, lys5::ade3::GAL10::HO, pRAD9-DPB11(292-600aa)-RAD9-3xFLAG::natMX, pADH1-DPB11(291-600aa)-RTT107(742aa-end)-6xHIS-3xHA::kanMX6*	This study
Y1912	*MATa ho hml::ADE1 hmr::ADE1 ade1-100 leu2-3, 112 lys5, trp1::hisG, ura3-52, lys5::ade3::GAL10::HO, slx4Δ::HPH*	(Dibitetto et al., 2016)
Y2437	*MATa ho hml::ADE1 hmr::ADE1 ade1-100 leu2-3, 112 lys5, trp1::hisG, ura3-52, lys5::ade3::GAL10::HO, slx4-7MUT-3xFlag::kanMX6*	Pellicioli's lab
Y1601 (YMV80)	*ho hml::ADE1 mata::hisG hmr::ADE1 his4::natMX leu2-(XhoI- to Asp718) leu2::MATa ade3::GAL::HO ade1 lys5 ura3-52 trp1*	Pellicioli's lab
Y3332	*ho hml::ADE1 mata::hisG hmr::ADE1 his4::natMX leu2-(XhoI- to Asp718) leu2::MATa ade3::GAL::HO ade1 lys5 ura3-52 trp1 pRAD9-DPB11(292-600aa)-RAD9-3xFLAG::kanMX6*	This study
Y3335	*ho hml::ADE1 mata::hisG hmr::ADE1 his4::natMX leu2-(XhoI- to Asp718) leu2::MATa ade3::GAL::HO pRAD9-dpb11-K544A(292-600aa)-RAD9-3xFLAG::kanMX6*	This study
Y3459	*MATa ho hml::ADE1 hmr::ADE1 ade1-100 leu2-3, 112 lys5, trp1::hisG, ura3-52, lys5::ade3::GAL10::HO, pRAD9-DPB11(292-600aa)-RAD9-3xFLAG::natMX, pSLX4-DPB11(291-600aa)-RTT107(742aa-end)-6xHIS-3xHA::kanMX6*	This study

Table S2. Plasmids used in this study.

Plasmid No.	Vector	Gene	Mutation	Tag	Reference
pMBS146	*pRS414*	-	-	-	S. Emr (Cornell University)
pMBS148	*pRS416*	-	-	-	S. Emr (Cornell University)
pMBS252	*pcDNA3*	*Human TOPBP1 (32aa-end)*	-	HA	This study
pMBS255	*pcDNA3*	-	-	HA	L. Qi (University of Michigan)
pMBS663	*pcDNA3*	*Human TOPBP1 (32aa-end)*	*R1314Q*	HA	This study
pMBS664	*pcDNA3*	*Human TOPBP1 (32aa-end)*	*K704A W711R*	HA	This study
pMBS667	*pcDNA3*	*Human TOPBP1 (32aa-end)*	*K154A K155A*	HA	This study
pMBS809	*pRS416*	*pADH1-MBD [dpb11(292-600aa)-rtt107(742aa-end) fusion]*	-	HA	(Cussiol et al., 2015*)*
pMBS825	*pFa6a*	*link-yomRuby2-kanMX6 (for mRuby2 epitope-tagging)*	-	-	C. Fromme (Cornell University)
pMBS910	*pRS414*	*pADH1- MBD [dpb11(292-600aa)-rtt107(742aa-end) fusion]*	-	HA	This study
pMBS912	*pRS416*	*pRAD9-dpb11(292-600aa)-RAD9*	-	FLAG	This study
pMBS913	*pRS416*	*pRAD9-dpb11 (292-600aa)-RAD9*	*K544A in dpb11 (292-600aa)*	FLAG	This study
pMBS924	*pFA6a*	*dpb11 (292-600aa)-RAD9*	-	FLAG	This study
pMBS925	*pFA6a*	*dpb11 (292-600aa)-RAD9*	*K544A in dpb11 (292-600aa)*	FLAG	This study
pMBS220	*pFA6a*	*slx4*	*T457A,T474A, S499A,T597A, S627A,S659A ,S725A*	FLAG	(Ohouo et al, 2010)
Addgene #11680	*pEGFP-N1*	*H2B*	-	EGFP	G. Wahl (Salk Institute)
AS159	*pHAGE-CMV-puro (gateway destination vector)*	-	-	FLAG-HA	A. Smogorzewska (Rockefeller University)
pYL81	*pHAGE-CMV-puro (gateway)*	*53BP1*	-	FLAG-HA	This study
pYL105	*pHAGE-CMV-puro*	*RFC1 (1-120aa)-53BP1*	-	FLAG-HA	This study
pMBS678	*pHAGE-CMV-puro*	*BRCA1*	-	FLAG-HA	This study

pMBS949	*pOG44 Flp Recombinase*	-	-	-	J. Baskin (Cornell University)
pMBS950	*pcDNA5/FRT/TO*	-	-	-	J. Baskin (Cornell University)
pMBS969	*pcDNA5/FRT/TO*	*RFC1 (1-120aa)-53BP1*	-	FLAG-HA	This Study
Addgene #26475	*pDR-GFP*	-	-	-	M. Jasin (Sloan Kettering Cancer Center)
Addgene #26477	*pCBASceI*	-	-	-	M. Jasin (Sloan Kettering Cancer Center)
pYL181	*pHAGE-CMV-puro*	*RFC1 (1-120aa)-53BP1*	*D1521R in 53BP1*	FLAG-HA	This Study
pYL185	*pHAGE-CMV-puro*	*RFC1 (1-120aa)-53BP1*	*R1627A in 53BP1*	FLAG-HA	This Study
pBABE HA–*Asi*SI–ER	*pBABE-puro*	*AsiSI–ER*	-	HA	(Iacovoni et al., 2010), G. Legube (Centre de Biologie Integrative, Toulouse)

Table S3. Mass spectrometry analysis of TOPBP1 interactions in HU. HEK293T cells grown in 'light' and 'heavy' SILAC DMEM media were treated with 1 mM HU for 24 h to identify proteins that interact with TOPBP1 in response to replication stress using quantitative mass spectrometry analysis. In the first experiment, TOPBP1 was purified from the 'light' HEK293T cells over-expressing HA-TOPBP1 using anti-HA agarose resin and the 'heavy' HEK293T cells transfected with empty vector were used as control. 'Light' and 'heavy' immunoprecipitated samples were then combined and subjected to quantitative mass spectrometry analysis. Proteins identified with 'light'/'heavy' ratios over 4 were considered as TOPBP1 interactor candidates. The log values of the ratios were listed in the second column below. In a second experiment, endogenous TOPBP1 in 'heavy' cells were purified using antibodies against TOPBP1 and the 'light' cells were immunoprecipitated using IgG. Similarly samples were analyzed by mass spectrometry and proteins with a 'heavy'/'light' ratio over 4 were considered as TOPBP1 interactor candidates. The log values of the ratios were listed in the third column below. Results from both experiment were then plotted on one scatter plot (Fig.4A) and combined. Proteins identified with a ratio over 4 in both experiments were designated as specific TOPBP1 interactors.

Protein	Log_2_gmean_HA (HA-TOPBP1/EV)	Log_2_gmean_antibody (anti-TOPBP1/IgG)	Sum of Log_2_gmean
FAM76B	9.1395	6.37412	15.51362
C12ORF32	7.06531	6.31639	13.3817
TOPBP1	5.2188	6.6847	11.9035
PARG	2.7971	7.93007	10.72717
C19ORF62	4.18129	5.77095	9.95224
BRCC3	5.50731	4.10167	9.60898
FAM175A	4.81326	4.69297	9.50623
USP34	3.60776	5.66083	9.26859
BRIP1	4.78406	4.45631	9.24037
BARD1	4.66464	4.49646	9.1611
BRE	4.19729	4.3122	8.50949
BRCA1	4.61669	3.49432	8.11101
UIMC1	3.44746	4.57485	8.02231
RFC1	4.28801	3.68687	7.97488
VPRBP	2.39743	4.731	7.12843
GINS2	4.66313	2.42857	7.0917
STUB1	4.30541	2.59218	6.89759
KIAA1524	4.05063	2.62183	6.67246
RBBP8	2.29078	4.10034	6.39112
GINS3	4.10811	2.03172	6.13983
RFC5	3.08786	3.03216	6.12002
RFC2	3.68102	2.41269	6.09371
HSPH1	3.29891	2.68872	5.98763
HUWE1	2.21355	2.91902	5.13257
APC	2.21562	2.81626	5.03188
HSPA1A,HSPA1B,HSPA6,HSPA7,HSPA1L	2.7535	2.15803	4.91153
ELP2	2.32399	2.49236	4.81635
GINS4	2.40012	2.19127	4.59139

Table S4. Mass spectrometry analysis of TOPBP1 interactions in nocodazole. Similar procedures were performed as described in Table S3 for cells treated with 100 ng/ml nocodazole for 14 h to define TOPBP1 interactions in G2/M.

Protein	Log_2_gmean_HA (HA-TOPBP1/EV)	Log_2_gmean_antibody (anti-TOPBP1/IgG)	Sum of Log_2_gmean
TOPBP1	6.35269	7.51805	13.87074
RFC1	4.00039	4.89725	8.89764
TP53BP1	3.89157	4.42037	8.31194
SIRT1	3.8237	4.07372	7.89742
PLK1	2.55711	5.12736	7.68447
USP28	2.79535	4.86396	7.65931
BRCA1	4.32419	2.82965	7.15384
RFC3	3.06349	4.01449	7.07798
RFC5	3.30205	3.52079	6.82284
SLX4	2.47809	3.9555	6.43359
RFC4	2.93517	3.48164	6.41681
RFC2	2.6685	3.64168	6.31018
HSPH1,HSPA4,HSPA4L	3.10754	2.79045	5.89799
BARD1	2.89024	2.90297	5.79321
UIMC1	2.13456	3.46231	5.59687
RPS4Y1,RPS4XP21,RPS4Y2,RPS4X	2.89016	2.59294	5.4831
PHF8	2.59627	2.87815	5.47442
HSPA1A,HSPA1B,HSPA6,HSPA7,HSPA1L	3.13207	2.17286	5.30493
SMARCAD1	2.97361	2.33108	5.30469
HSPA1A,HSPA1B	2.85148	2.43277	5.28425
HSPA1A,HSPA1B,HSPA1L	2.82783	2.41327	5.2411
HSPA1A,HSPA1B,HSPA6,HSPA7	2.83975	2.35702	5.19677
HSPA1A,HSPA1B,HSPA6,HSPA1L	2.68452	2.39823	5.08275
HSPH1	2.56549	2.42604	4.99153
STUB1	2.51056	2.45653	4.96709
HSPA1A,HSPA1B,HSPA6	2.50868	2.08801	4.59669
HSPA2,HSPA6,HSPA8	2.28422	2.21381	4.49803
HTATSF1	2.10301	2.38395	4.48696
HSPA2,HSPA1A,HSPA1B,HSPA6, HSPA7,HSPA8,HSPA1L	2.0546	2.17001	4.22461

Table S5. Mass spectrometry analysis of TOPBP1 interactions in HU versus nocodazole. HEK293T cells grown in 'heavy' and 'light' DMEM media were arrested with 1 mM HU for 24 h or with 100ng/ml nocodazole for 14 h, respectively. Endogenous TOPBP1 was purified using antibodies against TOPBP1 in both 'heavy' and 'light' lysates, which were combined and analyzed by mass spectrometer. TOPBP1 interactions defined in Tables S3 and S4 were monitored for changes in the experiment and ratios are listed below.

Protein	Log_2_gmean (HU/nocodazole)
BRIP1	3.40568
BRCA1	3.04482
BARD1	2.77511
BRE	1.04264
PARG	0.99916
C19ORF62	0.88487
BRCC3	0.63824
GINS2	0.61166
FAM175A	0.5862
UIMC1	0.53798
RBBP8	0.49421
RFC5	0.48059
ELP2	0.4713
SIRT1	0.43708
PHF8,PHF2	0.43109
C12ORF32	0.42731
RFC4	0.40272
RFC2	0.4002
RFC1	0.39062
RFC3	0.32742
STUB1	0.2183
GINS3	0.18872
GINS4	0.15367
HTATSF1	0.00876
TOPBP1	0.007
APC	-0.0568
PHF8	-0.06992
VPRBP	-0.09667
HSPA1A,HSPA1B	-0.19566
PLK1	-0.2281
HSPH1	-0.24604
HUWE1	-0.38979
SMARCAD1	-0.5129
KIAA1524	-0.85013
SLX4	-1.45355
USP28	-2.1004
TP53BP1	-2.20442

Table S6. List of oligonucleotides used for ChIP and DSB resection analysis in yeast.

Name	Sequence (5'-3')	Distance from DSB	Source
QMAT1.F	CCTGGTTTTGGTTTTGTAGAGTGG	0.15 kb (ChrIII)	(Ferrari et al., 2015)
QMAT1.R	GAGCAAGACGATGGGGAGTTTC	0.15 kb (ChrIII)	(Ferrari et al., 2015)
QMAT1.4kbF	ATTCCGTAAAGTCATAAGCACCCAC	1.4 kb (ChrIII)	This study
QMAT1.4kbR	GTCCGCAGCTTGATTGAAAATGTTG	1.4 kb (ChrIII)	This study
QMAT2.F	ATTGCGACAAGGCTTCACCC	4.8 kb (ChrIII)	(Ferrari et al., 2015)
QMAT2.R	CCACATCACAGGTTTATTGGTTCC	4.8 kb (ChrIII)	(Ferrari et al., 2015)
QPRE1.F	CCCACAAGTCCTCTGATTTACATTCG	Chr V	(Ferrari et al., 2015)
QPRE1.R	ATTCGATTGACAGGTGCTCCCTTTTC	Chr V	(Ferrari et al., 2015)

Table S7. List of oligonucleotides used for DSB resection analysis in human cell lines.

Primer Name	Sequence
DSB 335 FW	AATCGGATGTATGCGACTGA
DSB 335 RV	AAAGTTATTCCAACCCGATCC
DSB 1618 FW	TGAGGAGGTGACATTAGAACTCAGA
DSB 1618 RV	AGGACTCACTTACACGGCCTTT
Across DSB FW	GA TGTGGCCAGGGA TTGG
Across DSB RV	CACTCAAGCCCAACCCGT
No DSB FW	ATTGGGTATCTGCGTCTAGTGAGG
No DSB RV	GACTCAATTACATCCCTGCAGCT

References

Dibitetto, D., M. Ferrari, C.C. Rawal, A. Balint, T. Kim, Z. Zhang, M.B. Smolka, G.W. Brown, F. Marini, and A. Pellicioli. 2016. Slx4 and Rtt107 control checkpoint signalling and DNA resection at double-strand breaks. *Nucleic Acids Res*.

Ferrari, M., D. Dibitetto, G. De Gregorio, V.V. Eapen, C.C. Rawal, F. Lazzaro, M. Tsabar, F. Marini, J.E. Haber, and A. Pellicioli. 2015. Functional interplay between the 53BP1-ortholog Rad9 and the Mre11 complex regulates resection, end-tethering and repair of a double-strand break. *PLoS Genet*. 11:e1004928.

Iacovoni, J.S., P. Caron, I. Lassadi, E. Nicolas, L. Massip, D. Trouche, and G. Legube. 2010. High-resolution profiling of gammaH2AX around DNA double strand breaks in the mammalian genome. *EMBO J*. 29:1446-1457.

Ohouo, P.Y., F.M. Bastos de Oliveira, B.S. Almeida, and M.B. Smolka. 2010. DNA damage signaling recruits the Rtt107-Slx4 scaffolds via Dpb11 to mediate replication stress response. *Mol Cell*. 39:300-306.

Ohouo, P.Y., F.M. Bastos de Oliveira, Y. Liu, C.J. Ma, and M.B. Smolka. 2013. DNA-repair scaffolds dampen checkpoint signalling by counteracting the adaptor Rad9. *Nature*. 493:120-124.